IEEE Access
Multidisciplinary ⋮ Rapid Review ⋮ Open Access Journal

Received 16 August 2023, accepted 24 August 2023, date of publication 1 September 2023, date of current version 11 September 2023.

Digital Object Identifier 10.1109/ACCESS.2023.3311029

RESEARCH ARTICLE

Robust Variable Structure Control Approach of Two Series-Connected Five-Phase PMSMs Under Healthy and Faulty Operation Modes

ALI AJMI[1,2], SABER KRIM[2,3], ANISSA HOSSEYNI[1,2], MAJDI MANSOURI[4], (Senior Member, IEEE), AND MOHAMED FAOUZI MIMOUNI[1,2]

[1]National Engineering School of Monastir, University of Monastir, Monastir 5000, Tunisia
[2]Laboratory of Automatic, Electrical Systems and Environment (LASEE), National Engineering School of Monastir, University of Monastir, Monastir 5000, Tunisia
[3]Higher Institute of Applied Sciences and Technologies of Kasserine, University of Kairouan, Kairouan 3100, Tunisia
[4]Electrical and Computer Engineering Program, Texas A&M University at Qatar, Doha, Qatar

Corresponding author: Majdi Mansouri (majdi.mansouri@qatar.tamu.edu)

This work was supported by the Open Access funding provided by the Qatar National Library. The publication is the result of the Qatar National Research Fund (QNRF) Research Grant.

ABSTRACT In this paper a robust vector control method based on second order Super Twisting Sliding Mode Controllers (STSMCs) for two series-connected Five-Phase Permanent Magnet Synchronous Motors (FP-PMSMs) supplied by a single five-leg inverter is suggested. The vector control method of the two series-connected FP-PMSMs is based on six regulation loops for currents and speeds that are usually based on proportional integral controllers. Thus, the first aim of this paper is to replace the proportional integral controllers by the proposed second order STSMCs in order to enhance the control system performance in terms of robustness under uncertainties, external disturbances and tracking accuracy. Indeed, the second order STSMCs are proposed in order to overcome the limitations of the proportional integral controllers in terms of sensitivity against the variations in FP-PMSMs parameters and load disturbances and to overcome the first order sliding mode control chattering problem. However, the suggested second order STSMCs require information about the load torques applied to the two FP-PMSMs, which are estimated using sliding mode load torque observers hence reducing the cost and maintenance rate of the electromechanical system due to the elimination of load sensors. Our simulation studies conducted in MATLAB/Simulink check whether the proposed topology of the two series-connected FP-PMSMs controlled by the suggested vector control based on second order STSMCs can regulate the speed at the same time under various conditions. These conditions include load disturbances, parameter variations in both machines, and disturbances resulting from the opening of a phase. Our objective is to demonstrate the excellent robustness of the suggested second order STSMCs based vector control approach in terms of independent speed control of the two FP-PMSMs even at low or reversed speeds, compared with the conventional proportional integral control strategy. In this comparative study, various performance indices are used to demonstrate the robustness of the proposed vector control method based on second order STSMCs control strategy in comparison to the vector control method based on proportional integral controllers.

INDEX TERMS Five-phase PMSMs, vector control strategy, second order sliding mode control, supertwisting algorithm, faulty operation modes.

I. INTRODUCTION

In high-power industrial applications that require high operational reliability, unconventional structured electric machines provide an interesting solution. They are used in various

The associate editor coordinating the review of this manuscript and approving it for publication was Paolo Giangrande.

electromechanical systems such as electric propulsion in the field of railway traction, aerospace application [1], [2], electrical vehicles [3] and marine applications [4]. Unconventional structured electric machines refer to electric motor designs that differ from conventional configurations such as induction motors or synchronous motors. These machines can include configurations such as variable reluctance machines, axial flux machines, and Permanent Magnet Synchronous Motors (PMSMs). The PMSMs have become attractive due to their high power density, high efficiency, and low inertia [5]. The key advantage of these machines is their ability to meet the high-energy demands of mechanical loads. However, when high power is required, problems arise in terms of operational safety, acoustic discretization, and constraints on static switches in the inverter which need to switch high currents. Multiplying the number of phases allows, on the one hand, power segmentation, leading to a reduction in constraints on the components used in static converters. On the other hand, it enables a degraded operation while ensuring the continuity of service with low and acceptable torque ripples compared to three-phase machines [6]. This is particularly important in industrial applications where the failure of a propulsion system can have severe consequences in terms of safety, costs and operational efficiency. In PMSMs, the rotor excitation is provided by permanent magnets. Unlike other types of motors, PMSMs do not require an additional direct current power supply to ensure rotor excitation. This characteristic presents a significant advantage as it eliminates power losses associated with rotor windings and allows for a pseudo-linear Park model that is well suited for the real-time implementation of variable speed control structures. The rapid evolution of power electronics and control theory has enabled robust control of the multiphase electrical machines used in electric propulsion. These advances have contributed significantly to the replacement of mechanical propulsion due to their increased reliability [7]. In addition, these machines are generally lighter and more compact and they often have better dynamic characteristics than traditional mechanical propulsion solutions. Like multiphase electrical machines, some research work has dealt with different innovative topologies for controlling multiple machines connected in series or in parallel, thus reducing the weight without compromising performance [8], [9], [10], [11], [12]. To control the torque and flux of a multiphase system, generally only the direct (d) and quadrature (q) current components were used. The remaining current components could be allocated to control other machines fed by a single multi-leg inverter [13]. In a series connection topology, independent control of each machine would require specific coupling. However, it was important to consider an appropriate phase transposition when connecting. With proper phase transposition of the series connected machines, the current components produced independent control of each machine [14]. The torque ripples of one motor then depended on the speed of the other motor. These torque ripples severely degraded the efficiency of the system. In fact, a series connection of two PMSMs powered by a single five-leg inverter offers several advantages: Firstly, it reduces to half the number of transistors needed to control the motors. This results in a reduction in the investment costs and the overall system mass, which is particularly important in the aerospace and marine industries. In addition, independent control of the motors allows for better control of the speed and torque of each motor. This is particularly important in applications that require high precision or equal distribution of the load between different motors. This series topology can appear as an interesting application for electric propulsion in ships, even when both propellers are operated at reduced power and for different maneuvering modes, because it significantly reduces investment costs. This structure has been used for several years in the aerospace and maritime industries. Finally, the authors in [15] explored the advantages of this configuration and proposed solutions to improve system reliability and resilience. However, when a phase opening fault occurred in the inverter, the robust control of the inverter would allow the system to continue operating even with very small oscillations in the speeds of the two machines. This strategy produced good results with the drive studied in [15].

In this context and thanks to the benefits of the multiphase PMSMs and their operation in series connection, especially in the field of electric vehicles and ship driving, our research work is oriented towards the development of robust and high performance control of the aforementioned machines. Nevertheless, the application of the Vector Control (VC) strategy, proposed by Blascke in 1972, has been widely used for PMSMs where high-precision speed control in dynamic and static regimes is required [16], [17]. However, this control method is vulnerable to external disturbances and uncertainties related to parameters, since it uses Proportional Integral (PI) controllers. The PI controller performs well in a variety of industrial applications, but the main problem is that it is insufficient to counteract parameter changes and outside disturbances [18], [19], which subsequently impairs the system stability and dynamics. Indeed, in [20], the authors proposed an efficient control of two synchronous series-connected five-phase motors, which offered useful results. However, the two motors were controlled by a vector control method based on PI controllers. Moreover, the control technique performance was not evaluated under parameter variations and at very low speed ranges. In [10], the authors investigated a series connection of two five−phase permanent magnet synchronous motors supplied by a single inverter. Indeed, in the latter work, a decoupling control approach based on an improved dual−frequency vector modulation and a harmonic current compensation method was proposed to prevent the torque ripples. The performance of the proposed approach was verified by digital simulation and experimentation. However, the robustness performance of this approach is not verified since it used six control loops based on PI controllers. Moreover, PI controller offered limited performance and it seemed

unsuitable for controlling complex non-linear systems that operated under severe conditions, like the electric vehicle applications. Recently, the electric vehicles have gained increasing importance for several reasons, driven by environmental, economic and technological factors [21], [22], [23]. However, the complexity of electric vehicle operation the need to optimize their efficiency and range and the dynamic nature of driving conditions require robust control methods for electric motor management. These methods ensure that the vehicle performs efficiently, safely and predictably across a wide range of scenarios. In [21], the authors proposed a nonlinear robust H-infinity control technique for improving trajectory following performance of autonomous ground electric vehicles. To remedy the above-mentioned limitations of the PI controllers, several researchers have suggested different non-linear control approaches, such as the backstepping approach [24], the fuzzy logic control [25] the input-output linearization control [26], the adaptive control [27], the nonlinear robust H-infinity control [21], the robust finite frequency H_∞control strategy [22], Robust Vibration Control [23] and the Sliding Mode Control (SMC) [28].

Among the above-mentioned control techniques, the SMC technique is characterized by high performance in terms of excellent dynamics, rapid response and high durability in the face of changes affecting system parameters [29]. Consequently, effectively limiting these disturbances will be extremely difficult if linear control methods such as PI controllers are adopted [30]. Therefore, the SMC is a nonlinear control method renowned for its robustness under restricted disturbance conditions or in the presence of limited errors in the modeling of internal parameters, as well as for specific nonlinear behavior [31]. It should be noted that the main disadvantage of the SMC is the appearance of an undesirable effect known as ''chattering''. This phenomenon involves high-frequency oscillations that lead to unstable system dynamics, resulting in the loss of precision. To reduce the chattering phenomenon, researchers have proposed several solutions [32]. These include the use of functions smoother than the ''sign'' function, such as the hyperbolic tangent and the ''sat'' saturation functions [33]. Moreover, in [34], the authors proposed adaptive sliding mode control for five-phase PMSM. The suggested approach was well presented and it provided useful results. However, the chattering phenomenon was attenuated by replacing the ''sign(s)'' term by a term with softer variation related to saturation function ''sat(s)''. The use of the saturation functions reduced the phenomenon of chattering, but it could affect the precision of control [35].

In [36], a first order SMC was designed to regulate the speed of the five-phase salient-pole PMSM based on current measurements and estimations of the rotor speed and position. However, the chattering phenomenon was not investigated and the controller was tested only in a steady state operation and without parameter variations. Indeed, a new method was put forward in [37] to avoid chattering by modifying the non-linear component of the SMC with a new expression in order to reduce the chattering. Nevertheless, this method was applied to a three-phase induction motor; it was not tested at low speed ranges and under motor parameter variations. Similarly, extensive research has been conducted on the combination of a fuzzy inference system and SMC for multiphase machines in order to design a hybrid controller that would achieve better performance, calculate the constant used in the discontinuous component of control law in particular, and limit the chattering phenomenon [38]. Indeed, the fuzzy logic system was proposed to replace the discontinuous control action used in the conventional SMC technique which would reduce the chattering. However, the performance of the controller was not studied in details, since the operation at very a low speed, a locked rotor and under parameter robustness were not presented. In [39] and [40], the authors proposed several advanced controllers, such as the combination of nonlinear SMC and artificial neural networks. In [39] neural network combined with the SMC methodology was used to eliminate the chattering phenomenon and to improve the error performance of SMC for a multi-machine web winding system. This intelligent controller was tested within the criteria of speed overshoot and chattering reduction. However, the use of intelligent techniques considerably would increase the complexity of the control algorithm in terms of design and practical applications. In [41], the authors suggested improved Sliding Mode Reaching Law (SMRL) based field oriented control for a three-phase PMSM to reduce the sliding mode chattering. Indeed, according to the choice of a piecewise function term, the proposed SMRL adaptively selected the reaching velocity of the sliding mode. The authors demonstrated that the suggested SMRL offered satisfactory performance in steady state operations, but the rotor speed deviation when the load was applied would be higher and approximately equal to 200 rpm. Moreover, the authors in [42] proposed a fractional order SMC for the performance improved of a three-phase PMSM. This controller offered satisfactory performance in terms of speed tracking accuracy, but it used a high number of parameters for tuning. In the aforementioned paper, the authors introduced a neural network algorithm with reinforcement learning to determine the optimal parameters of the suggested controller, which offered better performance of control, but it increases the control system complexity.

To overcome the limitations of the aforementioned solutions, the Second-Order SMC (SOSMC) algorithms were proposed by Levant and other researchers [43], [44]. The most popular SOSMC used for controlling electrical systems and for observation were discussed by the authors in [45], which were the suboptimal algorithm, the prescribed convergence law algorithm, the quasi-continuous algorithm, the twisting algorithm and the super twisting algorithm. In the aforementioned paper, the SOSMC was used for controlling a five-phase interior PMSM, but the simulation results were insufficient to demonstrate the performance of the controlled

system in terms of accuracy, fast convergence, chattering reduction, etc. In [46], the authors put forward adaptive SOMC for multiple three-phase PMSM control systems. However, the SOSMC design required the calculation of the real-time higher-order derivatives of the outputs [47].

Among the control algorithms presented in [45], the super twisting algorithm was one of the most promising SOSMC algorithms.

Thus, the main advantages of STSMC include [48]: (*i*) compensation for Lipschitz perturbations/uncertainties, *(ii)* only information about the S sliding variable, *(iii)* requiring finite-time convergence to the origin for both S and the surface derivative $\dot{S}$ are simultaneously provided, and *(iv)*chattering reduction by continuous control signals. This algorithm is applied for controlling the rotor speed of three-phase induction machine when direct torque control is applied, and it provides satisfactory performance in terms of tracking accuracy and chattering attenuation [19]. In [49], the authors synthesized a speed controller with a super-twisting sliding-mode algorithm for a three-phase PMSM. The obtained results confirmed that the proposed controller offered satisfactory performance, but it was not tested under sever conditions like very low and reversal speeds, locked rotors or parameter variations. Thanks to its excellent robustness under uncertainty and non-linearity, the supertwisting SOSMC was applied for controlling electrical motor that driven electric vehicles [50]. Indeed, the authors studied the path-following control problem for four-wheel-independent-drive electric vehicles. They took into account modeling mistakes and complicated driving scenarios. A supertwisting SOSMC strategy was used to ensure the operational safety and robustness. In the same vein, the super twisting SOSMC could be considered as a promising solution for manufacturers for controlling electromechanical systems like electric vehicles [21], [22], [23].

In this context, the first contribution of our article consists in combining a Super-twisting SMC (STSMC) with a vector control strategy for two Five-Phase PMSMs (FP-PMSMs) connected in series and supplied by a single five-leg inverter. Referring to the previously published research work, this idea has not been investigated yet. Indeed, each control loop of speeds and currents based on a PI controller is replaced by the suggested STSMC, which improves consequently the performance of the control system in terms of robustness under load disturbances and stator resistance variations, chattering reduction, very fast convergence with excellent accuracy, and low torque ripples.

Moreover, the proposed STSMC of speeds for each machine requires the information about the load torques, which can be measured by torque sensors or estimated using an observer or estimator. However, the torque sensors used increase the system cost, the maintenance rate and the system complexity. In this context, the second contribution of this paper is to synthesize a robust Super-Twisting Load Torque Observers (ST-LTOs) to estimate the load torques for each FP-PMSM. Thus, the developed control schemes combine the functionalities of robust control and robust torque estimation of two series-connected FP-PMSMs.

To sum up, the main goals and contribution of this paper, for both theory and simulation studies, are summarized as follows:

1) A newly modified vector control scheme based on STSMCs for two FP-PMSMs connected in series and supplied by a single five-leg inverter is introduced. The advantages of the proposed control scheme is to improve the system performance in terms of robustness under load disturbances and stator resistance variations, chattering reduction, very fast convergence with excellent accuracy, prevented chattering, and reduced torque ripples. A single five-leg inverter instead of two inverters reduces the power system cost and power losses. In the literature, they used a two series-connected FP-PMSMs fed by a single five-leg voltage source inverter and utilized them with PI-based or SMC- based vector control, without applying super-twisting SMC.
2) Robust ST-LTOs is put forward for load torque estimation, which consequently reduces the system cost, the complexity of the control system and the maintenance rate by eliminating the load sensors. Up to our knowledge, this has been the first time to use ST-LTOs in the literature in the structure of two series-connected FP-PMSMs fed by a single five-leg voltage source
3) In simulation aspects, the proposed vector control strategy with STSMC and ST-LTOs are designed under Matlab/Simulink environment and shows excellent robustness under load torque disturbances, stator resistance variations and fast dynamic responses with excellent accuracy and acceptable performance under one phase opening.
4) A comparative study by numerous scenarios of simulation between the PI and the suggested STSMC is carried out. Concerning results, the suggested controller provides better performance using several criteria, such as: speed response time, speed overshoot, robustness under load disturbances and parameter variation, chattering and torque ripples, as well as the operation continuity under an open phase.

The rest of the paper can be organized as follows: In section II, the mathematical model of an FP-PMSM and a brief presentation of a VC strategy of a two series-connected FP-PMSM and a brief presentation of a VC strategy of a two series-connected FP-PMSMs are presented. In section III, the STSMC and sliding mode observers for the load torque are developed. In section IV, the simulation results are presented to test the performance of the suggested VC method based on synthesized STSMC. Finally, the paper is concluded in section 6.

II. FP-PMSM MODELING AND PRINCIPLE OF VC METHOD

A. MODELING OF SINGLE FIVE-PHASE PMSM

A synoptic representation of a five-phase PMSM is given in Figure.1, where the angle "$2\pi/5$" is the geometric angle between each two successive phases. In the (a, b, c, d, e) stationary reference frame, the voltage equation of the five-phase PMSM can be expressed as follows [6], [8]:

$$[V_{abcde}] = [R_s]\,[i_{abcde}] + \frac{d\,[\Phi_{abcde}]}{dt} \tag{1}$$

where R_s denotes the resistance, Φ_{abcde} is the stator flux linkage, L is the stator inductance, V_a, V_b, V_c, V_d, V_e,i_a, i_b, i_c, id and i_e are respectively the stator voltages and currents in the (a, b, c, d, e) axis.

$$\Phi_{abcde} = [L_s]\,i_{abcde} + e_k$$
$$[L_s] = \begin{pmatrix} L & M_1 & M_2 & M_2 & M_1 \\ M_1 & L & M_1 & M_2 & M_2 \\ M_2 & M_1 & L & M_1 & M_2 \\ M_1 & M_2 & M_2 & L & M_1 \\ M_1 & M_2 & M_2 & M_1 & L \end{pmatrix} \tag{2}$$

where "L" is the stator inductance e_k is the EMF induced in the k^{th} phase by the permanent magnet rotor, M_1 is the mutual inductance between two adjacent phases which are phase-shifted by an electrical angle of $\pm 2\pi/5$, and M_2 is the mutual inductance between two non-adjacent phases (electrical shift angle $\pm 4\pi/5$).

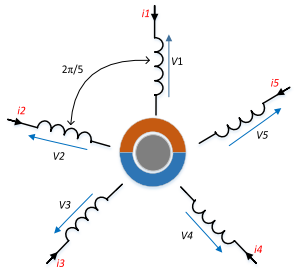

FIGURE 1. Illustration of FP-PMSM.

Modeling in the natural basis of the PMSM does not allow for an easy control model because of the strong magnetic coupling of the phases. It is interesting to exploit the symmetry and circularity of the inductance matrix to model the PMSM in a basis ensuring a magnetic decoupling of the phases. This new basis is obtained by applying a Concordia transform of order 5 defined as a matrix [C] of the passage from the natural basis to the decoupling basis defined in [20] and recalled in the appendix. The multi-phase machine is then split into several single-phase and fictitious two-phase machines, which are magnetically independent but mechanically coupled on the same shaft, which can be called main (plane α, β), secondary (plane x, y) and zero-sequence (h) [8].

This transformation results in:

$$\begin{cases} \vec{V}_{\alpha\beta} = R_s\,\vec{i}_{\alpha\beta} + L_P\left(\dfrac{d\,\vec{i}_{\alpha\beta-P}}{dt}\right) + \vec{e}_{\alpha\beta} \\ \vec{V}_{xy} = R_s\,\vec{i}_{xy} + L_s\left(\dfrac{d\,\vec{i}_{\alpha\beta-s}}{dt}\right) + \vec{e}_{xy} \\ \vec{V}_h = R_s\,\vec{i}_h + L_h\left(\dfrac{d\,\vec{i}_h}{dt}\right) + \vec{e}_h \end{cases} \tag{3}$$

The values of L_p and L_s can be calculated directly from L, M_1 and M_2. Their expressions are given by [8]:

$$\begin{aligned} L_p &= L + 2(M_1 cos(\frac{2\pi}{5}) + M_2 cos(\frac{4\pi}{5})) \\ L_s &= L + 2(M_1 cos(\frac{4\pi}{5}) + M_2 cos(\frac{2\pi}{5})) \end{aligned} \tag{4}$$

In order to express all quantities in the same reference frame, the application of Park's transformation leads to the following system of d-q equations [16]:

$$\begin{cases} Vd1 = R_s idp + L_p\dfrac{didp}{dt} - P\Omega L_p iqp \\ Vq1 = R_s iqp + L_p\dfrac{diqp}{dt} + P\Omega L_p idp + \sqrt{5/2}\,\omega_e \Phi_f \\ Vd3 = R_s ids + L_s\dfrac{dids}{dt} - 3P\Omega L_p iqs \\ Vq3 = R_s iqs + L_s\dfrac{diqs}{dt} + 3P\Omega L_s ids \end{cases} \tag{5}$$

where Φ_f, $P$and Ω denote the rotor flux created by the magnets and closed on the stator, the number of pair poles and the mechanical rotor speed, respectively.

Considering the mechanical load, the dynamic equation of the PMSM can be expressed as:

$$J\frac{d\Omega}{dt} = T_{em} - T_r - f\Omega \tag{6}$$

where T_{em} is the electromagnetic torque, T_r is the load torque, J is the moment of inertia and $f$is the friction coefficient.

B. SERIES-CONNECTED TOPOLOGY OF TWO FP-PMSMS WITH SINGLE 5-LEG VSI

For the system under study, two multi-phase machines connected in series are considered. No coupling is provided on the windings of the first machine, but the windings of the second machine are coupled in star. This series connection respects a particular phase transposition defined in [8] and [14] and shown in Figure 2. This connection leads to the possibility of independent control of both machines. The multi-phase power supply of the two machines is provided by a single five-arm inverter whose outputs are numbered by the capital letters *A, B, C, D*and *E*. On the other hand, the phase sequence of the two machines, respecting the spatial distribution of the windings (see Figure 1), is identified by the letters lower case *a, b, c, d* and *e*.

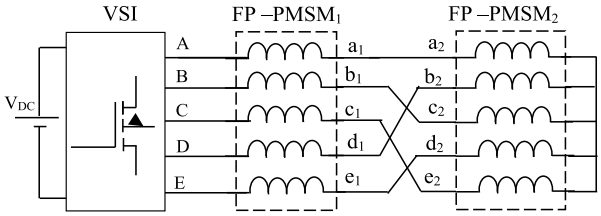

FIGURE 2. Topology of series-connected two five-phase PMSMs supplied by single inverter.

C. CASE OF TWO SERIES-CONNECTED PMSMS

To establish the equivalent model for the series connection of two FP-PMSMs, we start with the given model of a single FP-PMSM in equation (5). The modeling process involves transforming the system into different frames for analysis. First, we realize the equivalent model in the natural frame *abcde*. Next, we transform it into the α-β-x-y frames. Finally, we convert it into the d_1q_1-d_3q_3 frame. Considering the topology in Figure 1, the inverter output voltages, relative to the neutral point, are determined as the sum of the voltages across the windings of the two machines. The vector notation is as follows [14]:

$$[Vs] = \begin{bmatrix} V_A \\ V_B \\ V_C \\ V_D \\ V_E \end{bmatrix} = \begin{bmatrix} V_{a1} + V_{a2} \\ V_{b1} + V_{c2} \\ V_{c1} + V_{e2} \\ V_{d1} + V_{b2} \\ V_{e1} + V_{d2} \end{bmatrix} \tag{7}$$

The output currents of the inverter are given by:

$$\begin{aligned} i_A &= i_{a1} = i_{a2} \\ i_B &= i_{b1} = i_{c2} \\ i_C &= i_{c1} = i_{e2} \\ i_D &= i_{d1} = i_{b2} \\ i_E &= i_{e1} = i_{d2} \end{aligned} \tag{8}$$

Applying the Clark transformation matrix to the system in Figure 2 gives a new representation in the α-β-x-y frames:

$$\begin{bmatrix} V_\alpha^{inv} \\ V_\beta^{inv} \\ V_x^{inv} \\ V_y^{inv} \\ V_o^{inv} \end{bmatrix} = [C] \begin{bmatrix} V_{a1} + V_{a2} \\ V_{b1} + V_{c2} \\ V_{c1} + V_{e2} \\ V_{d1} + V_{b2} \\ V_{e1} + V_{d2} \end{bmatrix} = \begin{bmatrix} V_{\alpha 1} + V_{x2} \\ V_{\beta 1} - V_{y2} \\ V_{x1} + V_{\alpha 2} \\ V_{y1} + V_{\beta 2} \\ 0 \end{bmatrix} \tag{9}$$

The relationship between the output currents of the inverter and the currents of the two machines is expressed by:

$$\begin{cases} i_\alpha^{inv} = i_{\alpha 1} = i_{x2} \\ i_\beta^{inv} = i_{\beta 1} = -i_{y2} \\ i_x^{inv} = i_{x1} = i_{\alpha 2} \\ i_y^{inv} = i_{y1} = i_{\beta 2} \end{cases} \tag{10}$$

The new equation for the series connected substitution of equations (9) and (10) is given by:

$$\begin{cases} V_\alpha^{inv} = Ri_\alpha^{inv} + (L_{p1} + L_{s2})\dfrac{di_\alpha^{inv}}{dt} - \omega_{e1}\Phi_{f1}\sqrt{\dfrac{5}{2}}sin(\theta_1) \\ V_\beta^{inv} = Ri_\beta^{inv} + (L_{p1} + L_{s2})\dfrac{di_\beta^{inv}}{dt} - \omega_{e1}\Phi_{f1}\sqrt{\dfrac{5}{2}}cos(\theta_1) \\ V_x^{inv} = Ri_x^{inv} + (L_{s1} + L_{p2})\dfrac{di_x^{inv}}{dt} - \omega_{e2}\Phi_{f2}\sqrt{\dfrac{5}{2}}sin(\theta_2) \\ V_y^{inv} = Ri_y^{inv} + (L_{s1} + L_{p2})\dfrac{di_y^{inv}}{dt} + \omega_{e2}\Phi_{f2}\sqrt{\dfrac{5}{2}}cos(\theta_2) \end{cases} \tag{11}$$

where R_{s1} is added to R_{s2} to give a global resistance $R = R_{s1} + R_{s2}$. ω_{e1} and ω_{e2} denote the electric speeds for the FP-PMSM$_1$ and ω_{e2} for FP-PMSM$_2$.

The model obtained in equation (11) above followed by the Park transformation is a transformation into a two-phase system with two distinct rotations that are each defined by a sub matrix and grouped into the following matrix [P] that satisfies the special case of transposition.

$$[P] = \begin{bmatrix} cos(\theta_{e1}) & sin(\theta_{e1}) & 0 & 0 \\ -sin(\theta_{e1}) & cos(\theta_{e1}) & 0 & 0 \\ 0 & 0 & cos(\theta_{e2}) & sin(\theta_{e2}) \\ 0 & 0 & -sin(\theta_{e2}) & cos(\theta_{e2}) \end{bmatrix} \tag{12}$$

The application of the Park transformation leads to a system of d-q equations in which the current, the voltage and the EMF are constant. The angle θ_e in (12) is the instantaneous position of the rotor, which is different from the two machines and takes the value θ_{e1} for the first machine and θ_{e2} for the second [14]. The equivalent model of the series connection of the two PMSMs in the d-q frame is:

$$\begin{cases} V_d^{inv} = Ri_d^{inv} + (L_{p1} + L_{s2})\dfrac{di_d^{inv}}{dt} - \omega_{e1}(L_{p1} + L_{s2})i_q^{inv} \\ V_q^{inv} = Ri_q^{inv} + (L_{p1} + L_{s2})\dfrac{di_q^{inv}}{dt} + \omega_{e1}(L_{p1} + L_{s2})i_d^{inv} \\ \qquad + \Phi_{f1}\sqrt{\dfrac{5}{2}}\omega_{e1} \\ V_x^{inv} = Ri_x^{inv} + (L_{s1} + L_{p2})\dfrac{di_x^{inv}}{dt} - \omega_{e2}(L_{s1} + L_{p2})i_y^{inv} \\ V_y^{inv} = Ri_y^{inv} + (L_{s1} + L_{p2})\dfrac{di_y^{inv}}{dt} + \omega_{e2}(L_{s1} + L_{p2})i_x^{inv} \\ \qquad + \Phi_{f2}\sqrt{\dfrac{5}{2}}\omega_{e2} \end{cases} \tag{13}$$

where Φ_{f1} and Φ_{f2} are the total cash flow caused by the magnets and closed on stator *1* and stator *2*, respectively. The expressions of the electromagnetic torques are written as:

$$\begin{cases} T_{em1} = p_1\sqrt{5/2}.\Phi_{f1}.I_q \\ T_{em2} = p_2\sqrt{5/2}.\Phi_{f2}.I_y \end{cases} \tag{14}$$

Once again, we emphasize the independence of these two expressions: Each developed electromagnetic torque is

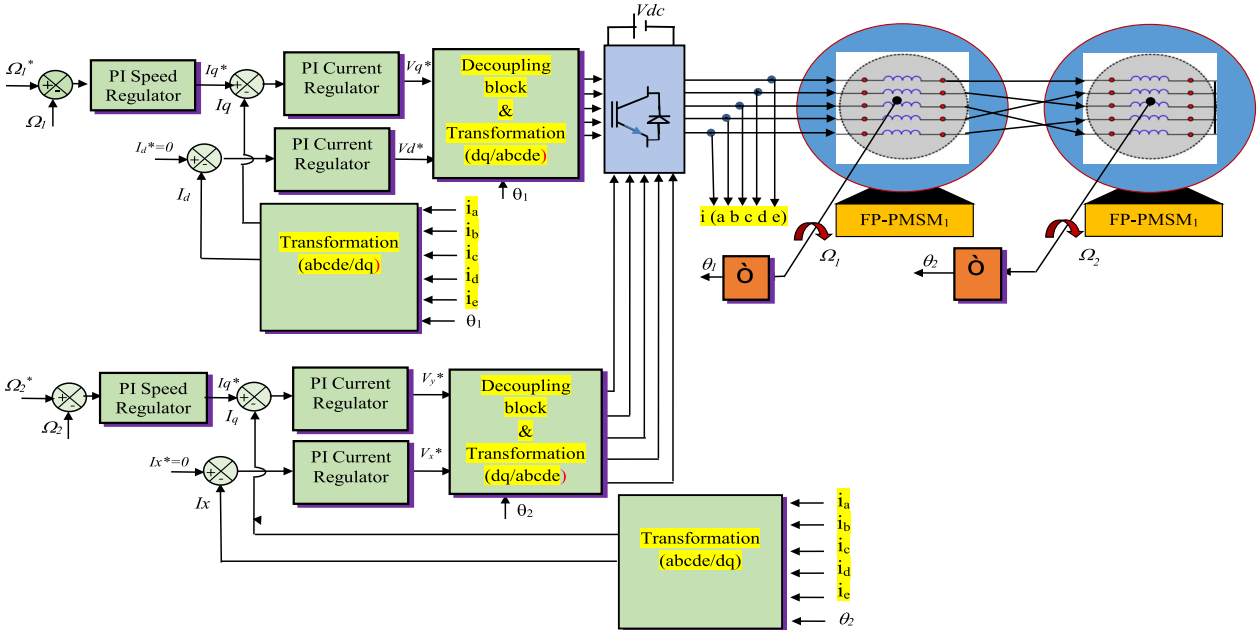

FIGURE 3. Block diagram of PI independent speed control of two series connected FP- PMSMs.

controlled exclusively by the current of its main fictitious machine: i_q for the first machine and i_y for the second machine.

D. VECTOR CONTROL OF TWO SERIES-CONNECTED FP-PMSMS

The drive system shown in Figure 2 consists of two FP-PMSMs fed by a single 5-leg voltage source inverter. Figure 2 illustrates the phase transposition rules for a series-connected system of two FP-PMSMs, where indices *1* and *2* identify the two machines. This particular transposition of stator windings enables the independent control of the two machines. Considering this series connection of the two machines (Fig. 2), the relationships between the inverter voltages and the voltages of each machine are as follows:

$$\begin{bmatrix} V_A^* \\ V_B^* \\ V_C^* \\ V_D^* \\ V_E^* \end{bmatrix} = \begin{bmatrix} V_{a1}^* + V_{a2}^* \\ V_{b1}^* + V_{c2}^* \\ V_{c1}^* + V_{e2}^* \\ V_{d1}^* + V_{b2}^* \\ V_{e1}^* + V_{d2}^* \end{bmatrix} \tag{15}$$

The inverter phase current references are given by:

$$\begin{bmatrix} i_A \\ i_B \\ i_C \\ i_D \\ i_E \end{bmatrix} = \begin{bmatrix} i_{a1} \\ i_{b1} \\ i_{c1} \\ i_{d1} \\ i_{e1} \end{bmatrix} = \begin{bmatrix} i_{a2} \\ i_{c2} \\ i_{e2} \\ i_{b2} \\ i_{d2} \end{bmatrix} = \begin{bmatrix} i_{a1}^* + i_{a2}^* \\ i_{b1}^* + i_{c2}^* \\ i_{c1}^* + i_{e2}^* \\ i_{d1}^* + i_{b2}^* \\ i_{e1}^* + i_{d2}^* \end{bmatrix} \tag{16}$$

Equations (13) and (14) are very independent, so we can control each machine separately. Among the used strategy is the vector control, based on PI controllers, where the i_d and i_x components are maintained at zero. We control the torques solely through the i_q and i_y currents. The overall voltage references are then provided by the current controllers according to the functional diagram of the vector control shown in Figure 3.

As shown in figure 3, the vector control strategy of the two series connected FP-PMSMs is based on six control loops based on a PI controllers. The calculation procedure of these controllers' parameters is detailed as follows:

1) SYNTHSIS OF SPEED CONTROLLER

The block diagram of the closed-loop speed controller is depicted in Figure 4. The speeds loop is implemented using a Proportional Integral (PI) controller, where the proportional coefficient is denoted as $k_{p\Omega j}$, (j=1, 2) of each machine, respectively.

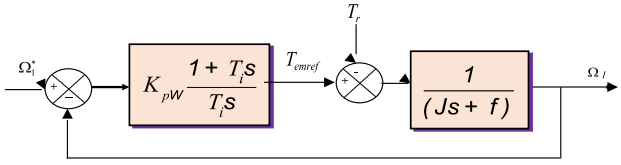

FIGURE 4. Block diagram of the closed-loop speed control.

The parameters of the speed controller are chosen to achieve the desired performance of the closed-loop system by specifying the damping ratio ζ and the natural frequency ω_0 [51], [52]. The speed control loops of FP-PMSM$_2$ are not discussed separately as they are essentially the same as FP-PMSM$_1$. The transfer function of closed loop G_{cl1} for

Figure 4 is given by:

$$G_{cl1} = \frac{\Omega_1}{\Omega_1^*} = \frac{1}{\frac{T_{i\Omega1}J_1}{K_{p\Omega1}}s^2 + T_{i\Omega1}(1 + \frac{f_1}{K_{p\Omega1}})s + 1} \tag{17}$$

The transfer function G_{cl1} exhibits a second-order dynamic response.

$$G_{cl1} = \frac{1}{\frac{1}{\omega_0^2}s^2 + \frac{2\xi}{\omega_0}s + 1} \tag{18}$$

By identifying the denominator of G_{cl1} in a canonical form of (18), we obtain the following relationships.

$$\begin{cases} \frac{1}{\omega_0^2} = \frac{T_{i\Omega1}J_1}{K_{p\Omega1}} \\ \frac{2\xi}{\omega_0} = T_{i\Omega1}(1 + \frac{f_1}{K_{p\Omega1}}) \end{cases} \tag{19}$$

To achieve a response without overshoot, the damping coefficient is set to $\zeta = 1$, which corresponds to the relation $\omega_0.t_{rep} = 4.75$, as provided in Table 5 in Appendix. Here, t_{rep} denotes the time for the speed response. Therefore, the parameters of the speed controller are determined as follows:

$$\begin{cases} T_{i\Omega1} = \frac{2J_1\omega_0 - f_1}{J_1\omega_0^2} \\ K_{p\Omega1} = 2J_1\omega_0 - f_1 \end{cases} \tag{20}$$

The output of the speed controller is the desired electromagnetic torque (reference torque), which is then multiplied by a constant k, to determine the reference q-axis current component. The reference currents for the d-axis (d), the direct-axis (x), and the q-axis (y) are maintained at zero. The parameter k can be expressed as:

$$k = \sqrt{\frac{2}{5}}\frac{1}{\Phi_{f_1}P_1} \tag{21}$$

2) SYNTHSIS OF CURRENTS CONTROLLERS

The current control loops are implemented in the (d, q); (x, y) frame. In this frame, the reference currents is continuous, allowing the use of PI controllers, which streamline the control process and enhance its efficiency. Figures 5 and 6 illustrate the block diagrams for the closed-loop current control along the (q, y) axis. As for the current models in (d, x), they are not discussed separately since they are essentially the same as the current loops in the (q, y) frame. The system involves two parameters that need to be determined:

- The PI controller of (d, q) axis current loop.
- The PI controller of (x, y) axis current loop.

As the current models are the same in the (d, q) axis and in the (x, y) axis, the two current controllers in the (d, q) axis, and the two current controllers in the (x, y) axis should be designed with the same integration time constant and the same proportionality coefficient, respectively. The proportional coefficients are k_{pp} and k_{pq} in the (d, q) axis and k_{px} and k_{py} in the (x, y) axis. The corresponding integral time constants in the (d, q) axis and (x, y) axis are respectively

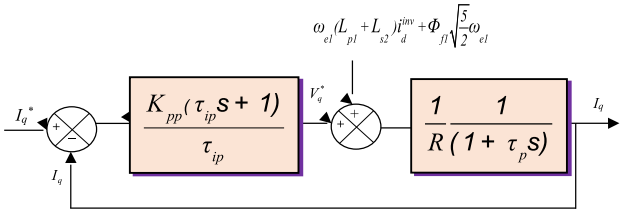

FIGURE 5. Block diagram of the closed loop Iq current control.

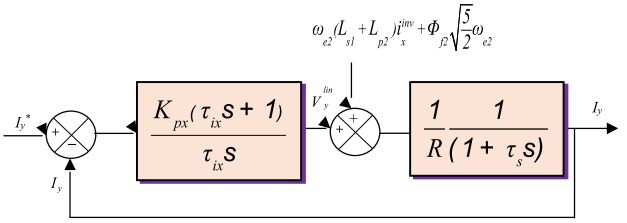

FIGURE 6. Block diagram of the closed loop Iy current control.

denoted as τ_{ip} and τ_{ix}. Consequently, the transfer functions of the PI controllers are as follows:

- In axis (d, q)

$$\frac{K_{pp}(\tau_{ip}s+1)}{\tau_{ip}s} \tag{22}$$

- in axis (x, y)

$$\frac{K_{px}(\tau_{ix}s+1)}{\tau_{ix}s} \tag{23}$$

The parameters of the PI current controllers are selected based on two criteria [53]: (1) ensuring that the zero of the current controller cancels the pole of the dominant time constant of the process, and (2) choosing a feedback loop time constant that is lower than that of the process.

The transfer function of the open loop for the current along the q axis is expressed as follows:

$$G_{qol} = \frac{K_{pp}(\tau_{ip}s+1)}{\tau_{ip}s}\frac{1}{R}\frac{1}{(1+\tau_p s)} \tag{24}$$

$\tau_p = \frac{L_{p1}+L_{s2}}{R}$ is the electrical time constant of the d - q axis current loop.

Considering the first rule

$$\tau_{ip}1 + 1 = 1 + \tau_p s \tag{25}$$

The simplified transfer function of the feedback loop system is:

$$G_{qcl} = \frac{1}{1 + R\frac{\tau_{ip}}{K_{pp}}s} = \frac{1}{1 + T_o s} \tag{26}$$

The time constant T0 of the feedback loop in the (d, q) axis current loop is set at a fixed value according to [52].

$$T_0 = R\frac{\tau_{ip}}{K_{pp}} = 0.116 * \tau_p \tag{27}$$

The integral time constant and the proportional coefficient of the PI current controller in the (d, q) axis are determined by solving equations (25) and (27).

Therefore, the parameters of the (d, q) axis current controller are given by:

$$\begin{cases} K_{pp} = \dfrac{R}{0.116} \\ \tau_{ip} = \tau_p \end{cases} \tag{28}$$

The y axis current is regulated by the previously described d-q axis current loop. Consequently, the integral time constant and the proportionality coefficient of the current controller in the x-y axis are determined by solving the following equations:

$$\begin{cases} \tau_{ix}s + 1 = 1 + \tau_s s \\ R\dfrac{\tau_{ix}}{K_{px}} = T_{0x} \end{cases} \tag{29}$$

$\tau_s = \dfrac{L_{s1} + L_{p2}}{R}$ is the electrical time constant of the x-y axis current loop. Additionally, the time constant T_{ox} of the feedback loop in the x-y axis current loop is fixed at a certain value.

$$T_{0x} = 0.116 * \tau_s \tag{30}$$

III. SLINDING MODE CONTROL OF SERIES-CONNECTED TWO FP-PMSMS

A. PRINCIPLE OF SMC

SMC is considered robust due to its inherent ability to maintain stable control in the presence of uncertainties, disturbances and variations in the system dynamics. The robustness of SMC is primarily attributed to the following key characteristics of the control technique [28], [45]:

✓ Sliding surface: SMC employs a sliding surface that guides the system state trajectory to track a desired reference trajectory. The sliding surface acts as a ''virtual wall'' that the system is forced to follow. This means that regardless of the system's inherent uncertainties or external disturbances, the control action is designed to keep the system state on this sliding surface.

✓ Discontinuous control action: SMC utilizes a discontinuous control law that switches the control action to keep the system on the sliding surface. This control action changes instantaneously, essentially ignoring small perturbations and focusing on maintaining the system on the sliding surface.

✓ Invariance principle: The fundamental idea behind SMC is the invariance principle, which states that if the system reaches the sliding surface, it will stay on it indefinitely. This invariance ensures that the system remains robust to uncertainties and disturbances, as it is designed to stay on the sliding surface despite external influences [48].

✓ Chattering: While chattering (rapid switching between control modes) is considered an undesirable feature of SMC, it contributes to the robustness of the control approach. Chattering helps counteract uncertainties and disturbances by rapidly adapting the control action to the changing dynamics of the system.

The SMC concept consists of three phases: an initial phase of reaching in which the state trajectory is driven to the surface S=0 and attains it in a finite time. This is succeeded by a sliding phase in which the trajectory slides on the switching surface to an equilibrium point. The fundamental principle of SMC is illustrated in Figure 7 [19].

The SMC principle is described by the following actions

i) Choice of a sliding surface.
ii) Determination of a control law u(x, t) that can attract all state trajectories towards the sliding surface in finite time.
iii) Maintaining the trajectory state around this surface using an appropriate switching logic

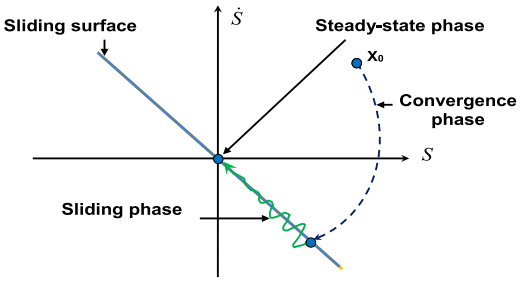

FIGURE 7. Different modes of SMC principle.

It is important to note that while SMC is robust to many types of uncertainties and disturbances, it may still have limitations or practical challenges, such as control chattering or sensitivity to high-frequency noise. Proper design and tuning of the control parameters are crucial to achieving the desired performance and Robustness in practical applications. The second order STSMCs is used in this paper to remove the chattering phenomenon without creating an accuracy problem, and at the same time save the main advantage of classical first- order SMC in terms of robustness against a very large class of uncertainties and/or perturbations.

In this study, the second-order STSMCs applied to the series-connected two PMSMs is twofold: to ensure a speed tracking according to the reference trajectory and to constrain the stator current components to their reference values, as in (31), shown at the bottom of the next page, where V_d, V_q, V_x, V_y and I_d, I_q, I_x and I_y are the voltage and current components of the main and secondary d and q axes. Equation (13) proves that the permanent magnet synchronous machine is a nonlinear multivariable system. In equation (31) I_d, I_q, I_x, I_y, Ω_1 and Ω_2 represent the state vector, and V_d, V_q Vx and Vy represent the control input vector.

The first step of the SMC design consists in defining a number of switching surfaces $S(x)$. In this paper we consider the following expression of the sliding surface [55], [56].

$$S(t) = \left(\frac{d}{dt} + \lambda\right)^{r-1} e(t) \tag{32}$$

where $e(x) = x - x_{ref}$ is the tracking error vector, λ is the positive constant and r denotes the relative degree and corresponds to the number of times that the surface needs to be differentiated before reaching the system input.

The second step consists in designing the control law to satisfy the condition $\dot{S}(x) = 0$ to ensure the convergence towards the sliding surface, and the attractiveness condition is given by:

$$S(X).\dot{S}(X) < 0 \tag{33}$$

To satisfy the convergence of the system state trajectories to the sliding surface $S(X) = 0$ in finite time, the discontinuons control action can be defined as follows [54].

$$U_n = K_i sgn(S(X)) \tag{34}$$

where K_i is a constant that must be chosen large enough to compensate for the disturbances of the system and for the difference between the output and its reference. It is important to note that the discontinuous nature of the control technique guarantees the robustness of the system to disturbances and uncertainties. The discontinuous term of the control law leads to the "chattering" phenomenon. A solution proposed to mitigate the effects of this phenomenon is to use a saturation function instead of the sign function, in order to achieve a smoother discontinuity [56], as illustrated in equation (35) and in Figure 8.

$$sat(S(X)) = \begin{cases} sgn(S(X)) & if\ |S(X)| > \delta \\ \dfrac{S(X)}{\delta} & if\ |S(X)| < \delta \end{cases} \tag{35}$$

where δ is the width of the boundary layer.

Remark: the saturation function provides better performance in terms of chattering attenuation, but the accuracy will be affected. Thus, the steady-state error will always exist. The problem of first order SMC can be solved using second-order STSMC, which will be synthesized in the following subsection.

B. PROPOSED SECOND-ORDER STSMC

The concept of higher-order SMC extends the idea of first- order SMC by using higher-order derivatives of the sliding surface. This approach maintains the same robustness and performance as SMC, but significantly reduces the chattering phenomenon [19], [46], [47], [48], [49], [50], [51], [52], [53], [54]. The objective of designing a super-twisting controller is to develop a suitable control law that enables the system control output to rapidly and accurately track the reference trajectory. This algorithm is capable of delivering a continuous control action using only the information on S. To determine the nth-order sliding mode, we must proceed as follows:

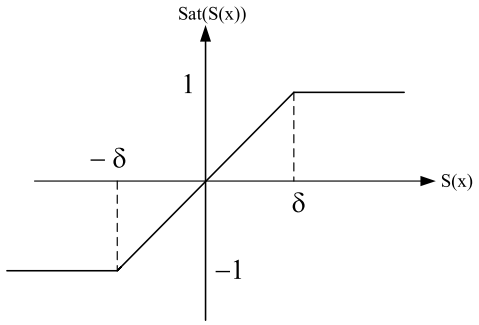

FIGURE 8. Saturation function.

$$S = \dot{S} = \ddot{S} = \ldots S^{(n-1)} = 0 \tag{36}$$

The second-order STSMC law integrates two parts. The first one is noted as "U_1" which includes a discontinuous time derivative function, while the second component, "U_2", represents a continuous function of the sliding variable [26], [55]. The continuous control law of the STSM in given as follows:

$$U_{ST} = U_1 + U_2 \tag{37}$$

with:

$$\begin{cases} U_1 = -\beta\sqrt{|S|}sgn(S) \\ \dot{U}_2 = -\gamma\, sgn(S) \end{cases} \tag{38}$$

The gain parameters of the control law, β and γ (both ≥ 0), are crucial. By adjusting these gains in an arbitrary manner,

$$\begin{bmatrix} \frac{di_d^{inv}}{dt} \\ \frac{di_q^{inv}}{dt} \\ \frac{di_x^{inv}}{dt} \\ \frac{di_y^{inv}}{dt} \\ \frac{d\Omega_1}{dt} \\ \frac{d\Omega_2}{dt} \end{bmatrix} = \begin{bmatrix} -\frac{R}{(L_{p1}+L_{s2})} i_d^{inv} + \omega_{e1} i_q^{inv} + \frac{1}{(L_{p1}+L_{s2})} V_d^{inv} \\ -\frac{R}{(L_{p1}+L_{s2})} i_q^{inv} - \omega_{e1} i_d^{inv} - \frac{\sqrt{5_{/2}}\omega_{e1}\Phi_{f1}}{(L_{p1}+L_{s2})} + \frac{1}{(L_{p1}+L_{s2})} V_q^{inv} \\ -\frac{R}{(L_{s1}+L_{p2})} i_x^{inv} + \omega_{e2} i_y^{inv} + \frac{1}{(L_{s1}+L_{p2})} V_x^{inv} \\ -\frac{R}{(L_{s1}+L_{p2})} i_y^{inv} - \omega_{e2} i_x^{inv} - \frac{\sqrt{5_{/2}}\omega_{e2}\Phi_{f2}}{(L_{s1}+L_{p2})} + \frac{1}{(L_{s1}+L_{p2})} V_y^{inv} \\ \frac{\sqrt{5_{/2}}P_1\Phi_{f1}}{J_1} i_q^{inv} - \frac{f}{J_1}\Omega_1 - \frac{1}{J_1} T_{r1} \\ \frac{\sqrt{5_{/2}}P_2\Phi_{f2}}{J_2} i_y^{inv} - \frac{f}{J_{12}}\Omega_2 - \frac{1}{J_2} T_{r2} \end{bmatrix} \tag{31}$$

limited time convergence can be achieved [55]. Generally, gain β has a stronger effect on the system response, while γ particularly affects the steady-state precision. The conditions required to ensure satisfactory finite-time convergence are outlined as follows [55]:

$$\begin{cases} \gamma > \dfrac{\phi}{\Gamma_{min}} \\ \beta^2 \geq \dfrac{4\phi\Gamma_{max}(\gamma+\phi)}{\Gamma_{min}^3(\gamma-\Phi)} \end{cases} \tag{39}$$

The positive bounds of the uncertain function Φ are defined byϕ. The positive upper and lower bounds of the uncertain function μ, which represents the second derivative of the sliding manifold, are represented by $\Gamma_{\min}$ and $\Gamma_{\max}$, respectively [26].

$$\Phi > \phi and\, \Gamma_{max} \geq \mu \geq \Gamma_{min} \tag{40}$$

$$\ddot{\Omega} = \phi(x,t) + \mu(x,t)\dot{u} \tag{41}$$

C. APPLICATION OF SECOND ORDER STSMC TO TWO FP-PMSMS

In this subsection a combination between the VC approach and second-order STSMC is presented. Thus, the PI controllers for the rotor speeds and currents are replaced by STSMC in order to perform a robust control strategy featured by high robustness under external disturbances, stator resistance variations and a chattering-free phenomenon. The different controllers will be synthesized below.

1) SYNTHESIS OF STSMC OF SPEEDS

In the present study, the error between the measured speeds and the reference ones for the two FP- PMSMs is chosen as the sliding mode surface, as given by the following expression [26]:

$$S(\Omega_j) = \Omega_j - \Omega_{jref}, \quad j = 1, 2 \tag{42}$$

By taking the time derivative of the sliding surface given by equation (42) and using the mechanical equations of the two machines, we obtain the following equations:

$$\begin{cases} \dot{S}_{\Omega 1} = \dot{\Omega}_1 - \dot{\Omega}_{1ref} = \dfrac{1}{J_1}(T_{em1} - f_1\Omega_1 - T_{r1}) - \dot{\Omega}_{1ref} \\ \dot{S}_{\Omega 2} = \dot{\Omega}_2 - \dot{\Omega}_{2ref} = \dfrac{1}{J_2}(T_{em2} - f_2\Omega_2 - T_{r2}) - \dot{\Omega}_{2ref} \end{cases} \tag{43}$$

where $T_{\rm rj}$, J_j, $\Omega_{\rm j}$ and f_j denote the load torque, the inertial value, the mechanical rotor speed and the damping coefficient of each machine, respectively.

From equation (43), equivalent control ensuring condition $\dot{S}_\Omega = 0$ gives:

$$\begin{cases} T_{em1eq} = J_1\,\dot{\Omega}_{1ref} + T_{r1} + f_1\Omega_1 \\ T_{em2eq} = J_2\,\dot{\Omega}_{2ref} + T_{r2} + f_2\Omega_2 \end{cases} \tag{44}$$

The reference torque produced by second-order SMC is expressed as follows:

$$\begin{cases} T_{em1ref} = T_{em1eq} + U_{ST1} \\ T_{em2ref} = T_{em2eq} + U_{ST2} \end{cases} \tag{45}$$

The equivalent control ensuring condition $\dot{S}_\Omega = 0$ gives the components of the equivalent control vectors $\mathrm{i}_{\rm qref}^{\rm inv}$ and $\mathrm{i}_{\rm yref}^{\rm inv}$ given by the following relation:

$$\begin{cases} i_{qref}^{inv} = \dfrac{(\dot{\Omega}_{1ref} + \frac{f_1}{J_1}\Omega_1 + \frac{1}{J_1}T_{r1})}{\frac{p_1\sqrt{5/2}\Phi_{f1}}{J_1}} \\ i_{yref}^{inv} = \dfrac{(\dot{\Omega}_{2ref} + \frac{f_2}{J_2}\Omega_2 + \frac{1}{J_2}T_{r2})}{\frac{p_2\sqrt{5/2}\Phi_{f2}}{J_2}} \end{cases} \tag{46}$$

To ensure finite-time convergence to the sliding surface, the control law is defined by:

$$\begin{cases} i_q^{inv} = i_{qref}^{inv} + U_{ST} \\ i_y^{inv} = i_{yref}^{inv} + U_{ST} \end{cases} \tag{47}$$

where $\mathrm{i}_{\rm qref}^{\rm inv}$ is defined in (46), and

$$U_{ST} = -k_1\sqrt{|S|}sgn(S) - \int_0^t k_2 sgn(S) \tag{48}$$

The expression of currents $\mathrm{i}_{\rm q}^{\rm inv}$ and $\mathrm{i}_{\rm y}^{\rm inv}$ have the following structure:

$$\begin{cases} i_q^{inv} = \dfrac{(\dot{\Omega}_{1ref} + \frac{f_1}{J_1}\Omega_1 + \frac{1}{J_1}T_{r1})}{\frac{p_1\sqrt{5/2}\Phi f_1}{J_1}} - \beta_{\Omega 1}\sqrt{|S_{\Omega 1}|}sgn(S_{\Omega 1}) \\ \qquad - \int_0^t \gamma_{\Omega 1} sgn(S_{\Omega 1}) \\ i_{yref}^{inv} = \dfrac{(\dot{\Omega}_{2ref} + \frac{f_2}{J_2}\Omega_2 + \frac{1}{J_2}T_{r2})}{\frac{p_2\sqrt{5/2}\Phi f_2}{J_2}} - \beta_{\Omega 2}\sqrt{|S_{\Omega 1}|}sgn(S_{\Omega 2}) \\ \qquad - \int_0^t \gamma_{\Omega 2} sgn(S_{\Omega 2}) \end{cases} \tag{49}$$

In order to investigate the stability of the switching surface, the generalized Lyapunov scalar function V(x, t) is employed, which is defined to be positive.

$$V(X) = \frac{1}{2}S^2(X) \tag{50}$$

The super twisting control law needs to satisfy the Lyapunov stability condition in order to ensure the stability of speed control. The time derivative of the Lyapunov function is characterized by:

$$\dot{S}(X).S(X) \prec 0 \tag{51}$$

By substituting, (45) in (43) we obtain:

$$\begin{cases} \dot{S}_{\Omega 1} = -\frac{1}{J_1}(\beta_{\Omega 1}\sqrt{|S_{\Omega 1}|}sgn(S_{\Omega 1}) + \int_0^t \gamma_{\Omega 1} sgn(S_{\Omega 1})dt) \\ \dot{S}_{\Omega 2} = -\frac{1}{J_2}(\beta_{\Omega 2}\sqrt{|S_{\Omega 2}|}sgn(S_{\Omega 2}) + \int_0^t \gamma_{\Omega 2} sgn(S_{\Omega 2})dt) \end{cases} \tag{52}$$

Subsequently, the Lyapunov stability condition can be expressed as follows:

$$\begin{cases} S_{\Omega 1}\dot{S}_{\Omega 1} = -\frac{S_{\Omega 1}}{J_1}(\beta_{\Omega 1}\sqrt{|S_{\Omega 1}|}sgn(S_{\Omega 1}) + \int_0^t \gamma_{\Omega 1} sgn(S_{\Omega 1})dt) \\ S_{\Omega 2}\dot{S}_{\Omega 2} = -\frac{S_{\Omega 2}}{J_2}(\beta_{\Omega 2}\sqrt{|S_{\Omega 2}|}sgn(S_{\Omega 2}) + \int_0^t \gamma_{\Omega 2} sgn(S_{\Omega 2})dt) \end{cases} \tag{53}$$

And it becomes:

$$\begin{cases} S_{\Omega 1}\dot{S}_{\Omega 1} = -\frac{\beta_{\Omega 1}}{J_1}|S_{\Omega 1}|^{\frac{3}{2}} sgn(S_{\Omega 1}) - S_{\Omega 1}\frac{\gamma_{\Omega 1}}{J_1}\int_0^t sgn(S_{\Omega 1})dt \\ S_{\Omega 2}\dot{S}_{\Omega 2} = -\frac{\beta_{\Omega 2}}{J_2}|S_{\Omega 2}|^{\frac{3}{2}} sgn(S_{\Omega 2}) - S_{\Omega 2}\frac{\gamma_{\Omega 2}}{J_2}\int_0^t sgn(S_{\Omega 2})dt \end{cases} \tag{54}$$

It is evident that both components of (54) are negative, provided that $\beta_{\Omega j}$ and $\gamma_{\Omega j} (j = 1, 2)$ are positive. As a result, the stability requirement is assured.

2) SYNTHESIS OF STSMCS OF CURRENTS

The goal of the control is to track the desired currents trajectories with excellent accuracy. Therefore, the sliding surfaces can be determined as follows:

$$\begin{cases} S(I_d) = I_d - I_{dref} \\ S(I_q) = I_q - I_{qref} \\ S(I_x) = I_x - I_{xref} \\ S(I_y) = I_y - I_{yref} \end{cases} \Rightarrow \begin{matrix} \dot{S}(I_d) = 0 \\ \dot{S}(I_q) = 0 \\ \dot{S}(I_x) = 0 \\ \dot{S}(I_y) = 0 \end{matrix} \tag{55}$$

Using equation (31), we can rewrite equation (55) as follows:

$$\begin{aligned} \dot{S}(I_d) &= -\frac{R}{(L_{p1}+L_{s2})}I_d^{inv} + \omega_{e1}I_q^{inv} + \frac{1}{(L_{p1}+L_{s2})}V_d^{inv} \\ &\quad - \dot{I}_{dref}^{inv} \\ \dot{S}(I_q) &= -\frac{R}{(L_{p1}+L_{s2})}1_q^{inv} - \omega_{e1}1_d^{inv} - \frac{\sqrt{5/2}\omega_{e1}\Phi_{f1}}{(L_{p1}+L_{s2})} \\ &\quad + \frac{1}{(L_{p1}+L_{s2})}V_q^{inv} - \dot{I}_{qref}^{inv} \\ \dot{S}(I_x) &= -\frac{R}{(L_{s1}+L_{p2})}I_x^{inv} + \omega_{e2}I_y^{inv} + \frac{1}{(L_{s1}+L_{p2})}V_x^{inv} \\ &\quad - \dot{I}_{xref}^{inv} \\ \dot{S}(I_y) &= -\frac{R}{(L_{s1}+L_{p2})}i_y^{inv} - \omega_{e2}i_x^{inv} - \frac{\sqrt{5/2}\omega_{e2}\Phi_{f2}}{(L_{s1}+L_{p2})} \\ &\quad + \frac{1}{(L_{s1}+L_{p2})}V_y^{inv} - \dot{I}_{yref}^{inv} \end{aligned} \tag{56}$$

Therefore, it is possible to select the control laws for the equivalent voltage reference as follows:

$$\begin{cases} V_{d\_eq}^{inv} = \frac{1}{(L_{p1}+L_{s2})}(\dot{I}_{dref}^{inv} - \omega_{e1}I_q^{inv} + \frac{R}{(L_{p1}+L_{s2})}I_d^{inv}) \\ V_{q\_eq}^{inv} = \frac{1}{(L_{p1}+L_{s2})}(\dot{I}_{qref}^{inv} + \omega_{e1}1_d^{inv} + \frac{\sqrt{5/2}\omega_{e1}\Phi_{f1}}{(L_{p1}+L_{s2})} \\ \qquad + \frac{R}{(L_{p1}+L_{s2})}1_q^{inv}) \\ V_{x\_eq}^{inv} = \frac{1}{(L_{s1}+L_{p2})}(\dot{I}_{xref}^{inv} - \omega_{e2}I_y^{inv} + \frac{R}{(L_{s1}+L_{p2})}I_x^{inv}) \\ V_{y\_eq}^{inv} = \frac{1}{(L_{s1}+L_{p2})}(\dot{I}_{yref}^{inv} + \omega_{e2}i_x^{inv} + \frac{\sqrt{5/2}\omega_{e2}\Phi_{f2}}{(L_{s1}+L_{p2})} \\ \qquad + - \frac{R}{(L_{s1}+L_{p2})}i_y^{inv}) \end{cases} \tag{57}$$

To ensure finite-time convergence to the sliding surface, the control law is defined by:

$$\begin{cases} V_d^{inv} = V_{d\_eq}^{inv} + U_{STd} \\ V_q^{inv} = V_{q\_eq}^{inv} + U_{STq} \\ V_x^{inv} = V_{x\_eq}^{inv} + U_{STx} \\ V_y^{inv} = V_{y\_eq}^{inv} + U_{STy} \end{cases} \tag{58}$$

where V_{d-eq}^{inv}, V_{q-eq}^{inv}, V_{x-eq}^{inv} and V_{y-eq}^{inv} are defined in (57). By replacing terms U_{STd}, U_{STq}, U_{STx} and U_{STy} by their expressions, equation (58) can be rewritten as follows:

$$\begin{cases} V_d^{inv} = V_{d\_eq}^{inv} - \beta_d\sqrt{|S_d|}sgn(S_d) - \int_0^t \gamma_d sgn(S_d) \\ V_q^{inv} = V_{q\_eq}^{inv} - \beta_q\sqrt{|S_q|}sgn(S_q) - \int_0^t \gamma_q sgn(S_q) \\ V_x^{inv} = V_{x\_eq}^{inv} - \beta_x\sqrt{|S_x|}sgn(S_x) - \int_0^t \gamma_x sgn(S_x) \\ V_y^{inv} = V_{y\_eq}^{inv} - \beta_y\sqrt{|S_y|}sgn(S_y) - \int_0^t \gamma_d sgn(S_y) \end{cases} \tag{59}$$

D. SYNTHESIS OF ST-LTO

The proposed ST-LTO system relies on load torque information, which is typically considered as an unknown variable. To get high performance in terms of accuracy, uncertainty reduction and tracking capability, it is recommended to employ a load torque observer based on the super-twisting

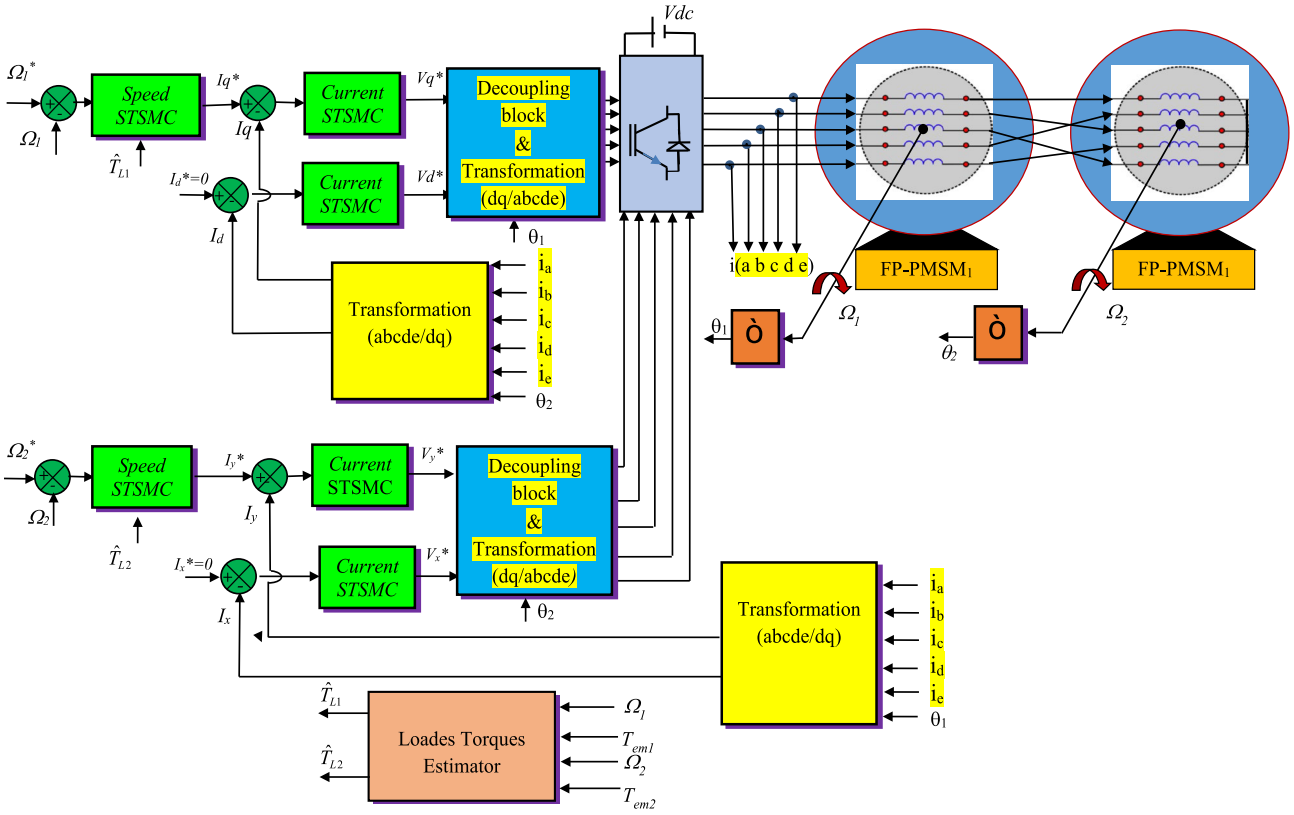

FIGURE 9. Block diagram of SMC of two FP- PMSMs connected in series.

algorithm. The mechanical equations of the two FP-PMSMs are given as follows:

$$\begin{cases} \hat{\Omega}_1 = \int (\frac{1}{J_1}(T_{em1} - T_{r1}) - \frac{f_1}{J_1}\Omega_1)dt \\ \hat{\Omega}_2 = \int (\frac{1}{J_2}(T_{em2} - T_{r2}) - \frac{f_2}{J_2}\Omega_2)dt \end{cases} \tag{60}$$

The sliding surfaces of the load torques can be represented as follows:

$$S_T(\Omega_j) = \widehat{\Omega}_j - \Omega_j, j = 1, 2 \tag{61}$$

For the FP-PMSM, the load torque can be estimated using equation (62) and equation (63), respectively of machine$_1$ and machine$_2$:

$$\begin{cases} \hat{T}_{l1} = \mu_T \left|S_{\Omega_1}\right|^{\frac{1}{2}} sign(S_T(\Omega_T)) + \hat{T}_{l11} \\ \dot{\hat{T}}_{l11} = \delta_T \, sign(S_T(\Omega_1)) \end{cases} \tag{62}$$

$$\begin{cases} \hat{T}_{l2} = \mu_T \left|S_{\Omega_2}\right|^{\frac{1}{2}} sign(S_T(\Omega_T)) + \hat{T}_{l22} \\ \dot{\hat{T}}_{l22} = \delta_T \, sign(S_T(\Omega_2)) \end{cases} \tag{63}$$

Finally, the suggested VC strategy based on both proposed STSMC and the ST-LTOs for FP-PMSMs connected in series, according to the transposition of Figure. 2, is given by Figure 9.

IV. SIMULATION RESULTS

This section presents the simulation study of two FP-PMSMs connected in series, supplied by a single five-leg inverter and controlled by a VC strategy based on PI controllers (VC-PI) and a VC strategy based on the suggested STSMC (VC- STSMC). The model of the power system and the control strategies is designed under a Matlab/Simulink environment. The solver used in the Simulink model is ode8 (DORMAND-Prince), with a sampling time of 50e–5. The parameters of the two FP-PMSMs are illustrated in Table 4. In order to evaluate the performance of the two control strategies, VC-PI and VC-STSMC, applied to the topology of two FP-PMSMs connected in series, various indices provide quantitative measures that reflect different aspects of performance. Moreover, other criteria are utilized for performance evaluation: (1) the Integral of Absolute Error (IAE), (2) the Integral of Squared Error (ISE) and (3) the Integral of Time multiplied by Absolute Error (ITAE).

The speeds errors are defined as:

$$\begin{cases} e_1 = \Omega_1 - \Omega_{1ref} \\ e_2 = \Omega_2 - \Omega_{2ref} \end{cases} \tag{64}$$

where Ω_{1ref} *and* Ω_{2ref} are the reference speeds for both machines, and Ω_1 *and* Ω_2 are the actual speeds of FP-PMSM$_1$ and FP-PMSM$_2$, respectively. *IAE*, *ISE* and *ITAE*are defined

as follows [55]:

$$\begin{cases} IAE = \int_0^t |e(t)|dt \\ ISE = \int_0^t e(t)^2 dt \\ ITAE = \int_0^t t\,|e(t)|dt \end{cases} \quad (65)$$

In order to illustrate the performance of both control strategies, different tests are performed for various operating scenarios. Therefore, the comparative study is conducted for four different modes as described below:

➢ **First scenario**

The main objective of this scenario is to test and analysis the performance of the suggested VC-STSMC in steady-state and reversal-speed operations. Indeed, the reference speeds of the two machines are identical and have a form of ramp, as given in Figure 10 (a, b). They increase slowly to reach 157 rad/s at t = 0.2s. Then they decrease at t=1s by applying a negative ramp that reaches −157 rad/s at t = 1.2s. We assume that both machines start at no load. After that, a load torque of 15 Nm is applied at t = 0.3s and then removed at t = 0.9s. Subsequently, a negative torque of −15 Nm is applied at t = 0.9s. Figure 10, Figure 11 and Figure 12 below show the corresponding simulation results.

Graphs (a), (b), (c) and (d) in Figure 10 show the rotor speeds responses and speed errors evolutions for PF-PMSM$_1$ and PF-PMSM$_2$, respectively. It can be seen that both control strategies perform well, ensuring good speed tracking. However, in this case, the variations in load torques are applied to both machines, gradually from 15 to −15 Nm, to evaluate the performance and robustness of control strategies with respect to the load variation in the drive system of two FP-PMSMs connected in series. However, in Figures 10(a)-(b), when the load torque is applied at t = 0.3 sec, it can be seen that when the machines are controlled by the VC method based on PI controllers, the rotor speeds present a larger steady-state errors, which are approximately equal to 3 rad/s for the FP-PMSM$_1$ and 3.8 rad/sec for the FP-PMSM$_2$. In contrast, when the two machines are controlled by the VC strategy based on STSMC, the rotor speeds present a low deviations which are evaluated by 1.6 rad/sec for the FP-PMSM$_1$ and 1 rad/sec for the FP-PMSM$_2$, which consequently demonstrate the robustness of the suggested second order STSMC under load disturbances.

Furthermore, in transient regime the dynamic speeds errors are equation to 3.144 rad/sec and 3.95 rad/sec when both machines are controlled by VC based on PI controllers. However, the dynamic error is neglected when the proposed VC based STSMCs is employed, as illustrated in Figure 10 (c, d). This means that the motors effectively and promptly respond to the load, adjusting their speeds to reach the desired values with excellent accuracy without any undesirable oscillations or overshooting. In the same context, the VC-PI approach results in a longer recovery time for the speeds of the FP-PMSM$_1$ and FP-PMSM$_2$ when the load torques are applied, which are approximately equal to 4.8ms and 5.7ms, respectively. This implies that the VC-PI approach requires more time for the motors to reach their reference speed after the application of the load torque. Additionally, it is mentioned that the VC-PI approach leads to overshooting, which means that the speeds can temporarily exceed the reference value before stabilizing. This can be undesirable in certain applications. When the load is removed at t = 0.9 s, the VC-STSMC approach results in a very low overshoot of 0.7 rad/s for FP-PMSM1 and 0.4 rad/s for FP-PMSM$_2$. This represents a significant reduction in overshoot compared to the PI approach, which is approximately 3.5 rad/s, with a reduction rate of about 75%. During load variations, the STSMC controllers keep the speeds close to their reference values, avoiding significant overshooting or drops. Therefore, it can be concluded that the STSMC exhibits greater robustness in the face of load variations. We also observe in Figure 10 (a)-(b) a very fast rise time for the STSMC, compared with the PI controller. This highlights the enhanced tracking precision achieved through the STSMCs approach and suggests potential avenues for further performance improvement. Consequently, it can be considered that the STSMC is more robust in the face of load variations.

Figure 11 shows the torque evolution of the two machines: FP-PMSM$_1$ and FP-PMSM$_2$. The torque of each machine remains constant, as depicted in Figure 11(a) and 11(b) using both PI and STSMC based-VC strategies. It is clear that the torque ripples for the STSMC have lower levels than those of the PI controller. Moreover, referring to the figure it can be seen that the estimated load torque converges perfectly towards the applied load, which proves that the synthesized ST-LTO operates well. To sum up, there is remarkable consistency between the measured and estimated load torques during both steady-state and transient operations.

Figure 12 depicts the converter current waveforms for the two proposed control strategies, VC-PI and VC-STSMC. It can be observed that all five inverter currents exhibit perfect sinusoidal behavior, attributed to both machines being driven at the same speed. It is clear that the sine wave of the current for the STSMCs is better compared with the one using the PI, as shown in Figure 12(a, b). However, the currents under the VC-STSMC control exhibit a smoother waveform, resulting in reduced copper losses compared to the VC-PI control, as illustrated in Figure 12(a). The PI controller exhibits waveforms with higher harmonics and a higher starting current, leading to an increase in the copper losses in comparison to the STSMCs. In addition, as presented in Figure 13(b), the Total Harmonic Distortion (THD), when the machines are controlled by the suggested VC-STSMC is equal to 0.32%. However, the THD is equal to 5.16% when the machines are controlled by the VC-PI as depicted in Figure 13(d).

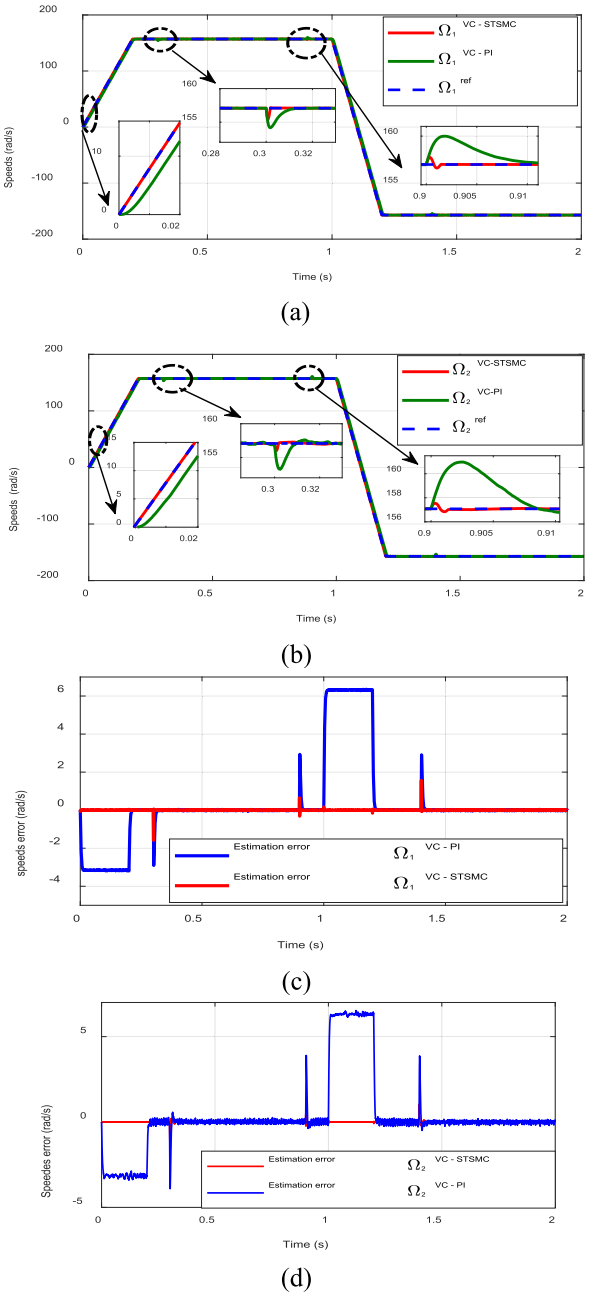

FIGURE 10. Comparative study between VC-STSMC and VC-PI controllers: (a) Speed of FP-PMSM1; (b) Speed of second FP-PMSM2; (c) Speed error for FP-PMSM1; (d) Speed error for FP-PMSM2.

Hence, thanks to the suggested VC-STSMC performance, a reduction rate of around 93.8% is gained.

Figure 13(a) shows that the current i_a at the converter output under STSMC is smoother than the current delivered under VC-PI, which has a high distortion rate as illustrated in Figure 13(a). Moreover, the proposed VC-STSMC strategy exhibits better performance indices such as IAE, ISE and ITAE, which demonstrates its superiority compared to the VC-PI strategy, resulting in an almost 100% performance improvement.

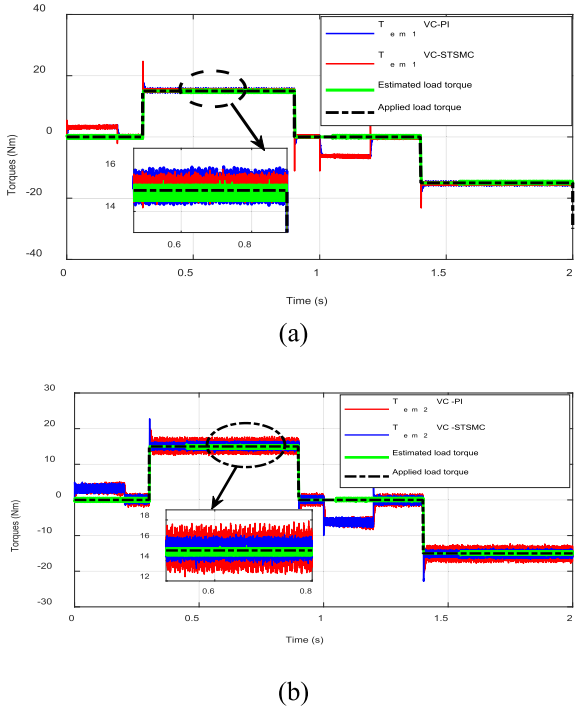

FIGURE 11. Comparative study between VC-STSMC and VC-PI controllers: (a) Electromagnetic torque, load torque and estimated load torque for FP-PMSM1; (b) Electromagnetic torque, load torque and estimated load torques for FP-PMSM2.

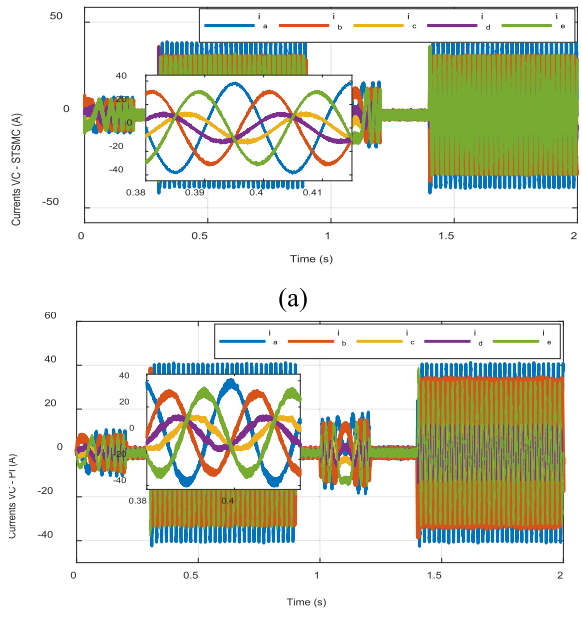

FIGURE 12. Comparative study between STSMC and PI controllers: (b) Current in five phases of voltage source inverter under VC-STSMC, (b) Current in five phase inverter under VC-PI.

More accurate comparison between the two control strategies VC-PI and VC-STSMC, in a healthy mode for controlling FP-PMSM1 and FP-PMSM2 connected in series is given in Table 1.

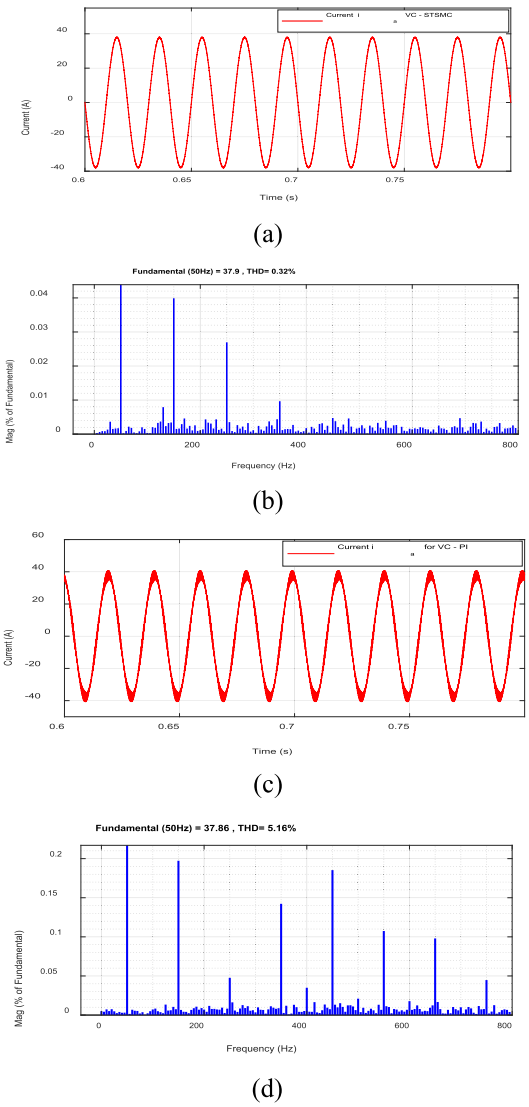

FIGURE 13. Comparative study between STSMC and PI controllers: (a) Closer observation of inverter current under VC-STSMC; (b) Closer observation of inverter current under VC-PI; (c) Inverter current harmonics spectrum under VC-STSMC; (d) Inverter current harmonics spectrum under VC-PI.

TABLE 1. Performance analysis of proposed VC-STSMC in steady state operation.

Controlled variables	Comparison criteria	VC-PI	The suggested VC-STSMC	Gain in (%) using STSMC
Speed and torque responses for FP-PMSM$_1$	Time deley to reach reference speed (ms)	4.8	Neglected	100
	Speed deviation when load is applied (rad/s)	3	1.6	46.67
	Recovery time when load is applied (ms)	18	2	88.9
	Overshoot when load is removed (rad/s)	2.9	0.7	75.86
	Dynamic speed error (rad/s)	3.144	0	100
	Torque ripples (%)	10.73	5.98	44.26
	ITAE	1.503	0.0046	99.69
	IAE	1.945	0.00519	99.73
	ISE	9.932	0.00425	99.95
Speed and torque responses for FP-PMSM$_2$	Time deley to reach reference speed (ms)	5.7	Neglected	100
	Speed deviation when load is applied (rad/s)	3.8	1	73.68
	Recovery time when load is applied (ms)	30	6.4	78.67
	Overshoot when load is removed (rad/s)	3.9	0.4	88.74
	Dynamic speed error (rad/s)	-3.95	0	100
	Torque ripples (%)	30.26	13.2	58.38
	ITAE	1.514	0.00365	99.75
	ITAE	1.954	0.00407	99.79
	ISE	9.94	0.00207	99.97
Inverter current	THD (%)	5.16	0.32	93.8

➢ Second scenario

The main objective of this scenario is to analyze the performance of the suggested VC-STSMC when the two machines operate independently and under different speeds. Thus, in this scenario the mechanical speed reference signals and the load torques applied to the two machines have different profiles. Initially, for FP-PMSM$_1$, a positive ramp is applied at t=0s, reaching a value of 157 rad/s at t=0.2s. At t=1.2s, the rotation speed is decreased slowly to reach 78.53 rad/s at t=1.4s. For the FP-PMSM$_2$, a positive ramp is applied at t=0s, reaching a value of 104.71 rad/s at t=0.2s. To validate the robustness of the VC-PI and VC-STSMC strategies, particularly during the locked rotor at t=1.4 s, the speed reference for FP-PMSM$_2$ is canceled, while FP-PMSM$_1$ continues to operate at a speed equal to 78.53 rad/s. For all simulation, we assume that both machines start at no load. Next, a load torque equal to 15 Nm at t =0.4s is applied to FP-PMSM$_1$ and a load torque of 12 Nm at t =0.6s is applied to the second machine FP-PMSM$_2$. The corresponding simulation results are given in Figure 14.

Figure.14 confirms the effectiveness of two control strategies and clearly shows that the two FP-PMSMs are much decoupled. Indeed, as shown in Figure 14(a), the speed of the second machine FP-PMSM$_2$ is not influenced by the variations in the speed of the first machine FP-PMSM$_1$, and vice versa. As presented in Figure 14(b), changes in the speed of the second machine have no impact on the torque quality of the first machine.

In addition, the VC-PI approach results in a longer recovery time under load application for the FP-PMSM$_1$ speed by around 15ms, and around 27ms for FP-PMSM$_2$, as illustrated in Figure 14 (a). For the VC-STSMC strategy, this time is very

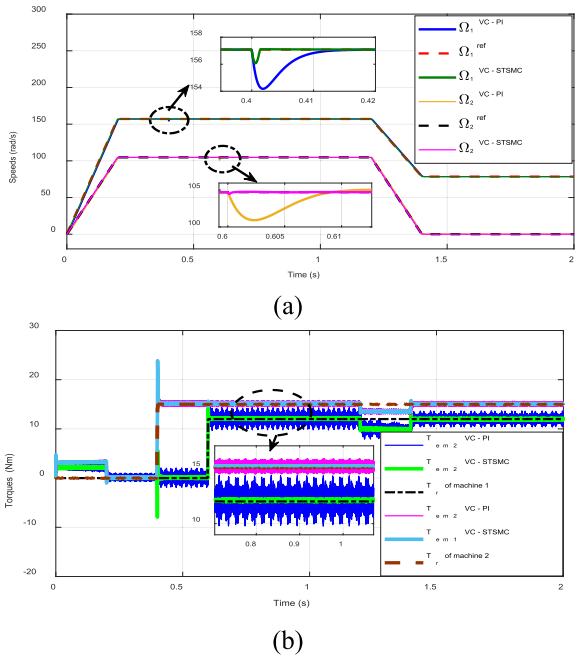

FIGURE 14. Comparative study between STSMC and PI controllers: (a) Speed of FP-PMSM1 and speed of FP-PMSM2, (b) Electromagnetic torque, load torque and estimated load torque for the both machines.

TABLE 2. VC-STSMC performance analysis with two different speed operations.

Controlled variables	Comparison criteria	VC-PI	VC-STSMC	Gain in %
Speed and torque responses for FP-PMSM$_1$	Time delay to reach reference speed (ms)	8.8	Neglected	100
	Speed deviation when load is applied (rad/s)	2.9	1	65.51
	Recovery time when load is applied (ms)	15	1.4	90,67
	Dynamic speed error (rad/s)	-3.144	0	100
	Torque ripples (%)	4.15	1.76	57.6
Speed and torque responses for FP-PMSM$_2$	Time delay to reach the reference speed (ms)	6.5	Neglected	100
	Speed deviation when load is applied (rad/s)	3.8	0.2	94.73
	Recovery time when load is applied (ms)	27	0.5	98.14
	Dynamic speed error (rad/s)	-3.95	0	100
	Torque ripples (%)	16.08	3.22	79.98

low, which is approximately equal to 1.4 ms for FP-PMSM$_1$ and 0.5ms for FP-PMSM$_2$, i.e. a gain of around 95%. Torques remain constant and follow their new references well. It is worth noting that the torque ripples are significantly lower for the VC-STSMC approach, compared to the VC-PI control approach. In addition, it can be seen that the load torques estimated using the ST-LTO closely follow the variations in the applied load torque for each machine. A more accurate comparison between the VC-PI and VC-STSMC strategies of FP-PMSM$_1$ and FP-PMSM$_2$ connected in series and operating under two different speeds is given in Table 2.

➢ Third scenario

The main goals of the scenario is to test the low-speeds and the high-torque performance of both VC-STSMC and VC-PI control strategies, on the topology under study. Figure 15 depicts the simulation results obtained. The stator resistances of both machines are increased to 100% of their nominal value at time t=0.8s and t=1.6s, as given in Figure 15(a). The load torques applied to both machines are equal to 12 Nm (60 c/o T_n). The graphs in (b) and (c) successively represent the temporal evolution of the speed and torque, for starting the motors at no load, followed by the application of the load torque at t=0.25s. The speed set points are considered as ramps, reaching 1.047 rad/s (10 rpm) for the first machine and 1.57 rad/s (15rpm) for the second machine at time t=0.1s.

Referring to Figure 15(b), it can be seen that when the load torque is applied, the VC-PI offers poor performance demonstrated by speed undershoot that reaches -2.44 rad/sec and is considered as a reversal of the speed direction, which indicates that the VC-PI strategy is not recommended at low speeds as it fails to keep stable and consistent torques and speeds under such conditions. However, when both machines are controlled by the suggested VC-STSMC, the rotor speeds present low undershoot and return to their references, so the latter suggested control method is robust load disturbances even at low speed operations. Furthermore, it is capable of maintaining stable speeds and torques and providing accurate responses even during load applications.

Moreover, the developed electromagnetic torques when the two machines are controlled by the control strategies is illustrated in Figure 15(c). In fact, referring to this figure it can be seen that the load torques present additional ripples when the VC-PI is employed, but the torque curves are smoother with low ripples when the suggested control technique is used, which improves the control quality and increases the service life of FP-PMSMs.

In the same context, the suggested VC-STSMC strategy is featured by good robustness under stator resistance variations, as depicted in Figure 15(b, c). Unlike the VC-PI, it can be seen that the deviations caused by the stator resistance variations on the rotor speeds and the torques for the two machines are low.

Compared to the VC–PI, VC-STSMC exhibits superiority in terms of overshoot magnitude and settling time. These results indicate that this parameter variation has no influence on the decoupling between the two machines. However, its impact on speeds, which are not so significant, has been quickly recovered thanks to the robustness of the VC-STSMC. More comparison and details are illustrated in Table 3.

➢ Fourth scenario

The main objective of this scenario is to analyze the behavior of two series-connected FP-PMSMs under faulty conditions described by one open phase, using two control strategies: VC-STSMC and VC-PI. Different mechanical speed

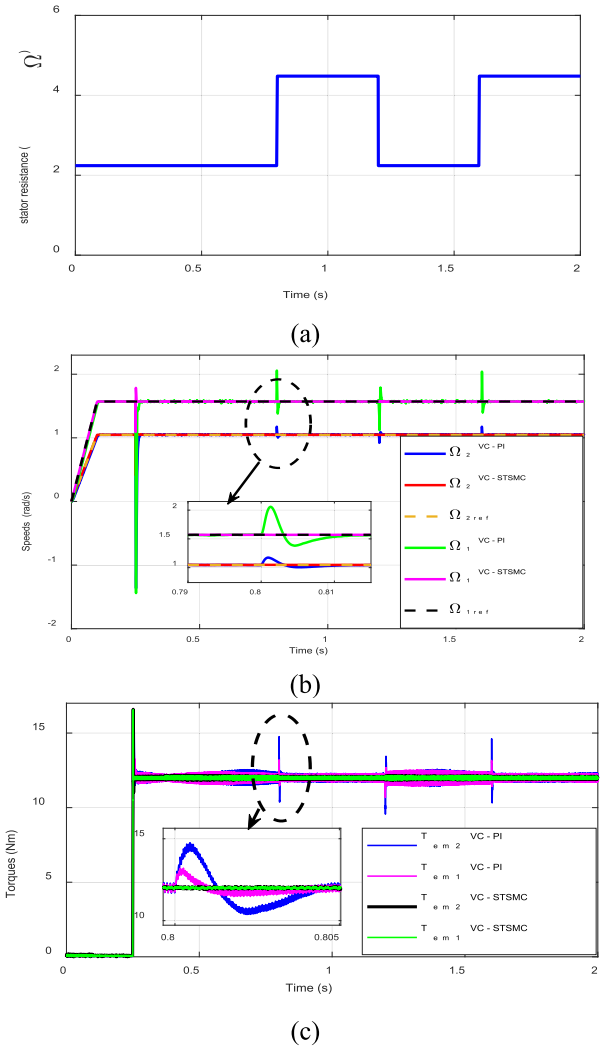

FIGURE 15. Sensitivity of control techniques VC-PI and VC-STSMC to variation in stator resistances at low speed and high torque: (a) Stator resistance variation; (b) Speeds; (c) Electromagnetic torques.

reference profiles are applied to both machines in the presence of a stator phase opening. For the first machine, a positive ramp starts at t=0, reaching a value of 157 rad/s (1500 rpm) at t=0.2s. For the second machine, a positive ramp starts at t=0, reaching a value of 104.72 rad/s (1000 rpm) at t=0.2s. At t=1s, an opening fault of phase1 occurs in the inverter that supplies power to both machines. Figures 16 illustrates the temporal evolution of the electrical and mechanical quantities of both FP-PMSMs. For all simulation, we assume that the two machines start at no load. Then we apply a load torque of 15 Nm at t =0.4s for FP-PMSM$_1$ and 12 Nm at t =0.6s for FP-PMSM$_2$.

Figure 16 (c) shows the temporal evolution of the rotor speeds for the two control strategies. For the VC-PI, we see a divergence of speeds from the target-operating regime, with a loss of stability. When the machines are controlled by the suggested VC-STSMC method, it can be seen that both rotor

TABLE 3. Robustness evaluation at low speed operations.

Controlled variables	Comparison criteria	VC-PI	VC-STSMC	Gain in %
Speed and torque responses for FP-PMSM$_1$	Speed deviation when load is applied (rad/s)	3	0.477	84.1
	Speed overshoot when stator resistance increased or decresed	0.483	0	100
	Torque deviation when stator resistance changed (rad/s) (max-min)	1.4	0.12	91.42
	Torque ripples (%)	7.16	2.08	70.94
	Robustness	poor	excelent	100
Speed and torque responses for FP-PMSM$_2$	Speed deviation when load is applied (rad/s)	2,407	0.58	75,9
	Speed overshoot when the stator resistance increased or decresed	0.127	0	100
	Torque deviation when the stator resistance changed (rad/s) (max-min)	4.31	0.11	97.44
	Torque ripples (%)	8.33	1.91	77
	Robustness	poor	excelent	100

speeds exhibit very low oscillations maintained around the steady state with no loss of static stability. Graphs (a) and (b) in Figure 16 show that the electromagnetic torques are highly oscillatory, with severe, negative torque oscillations and peaks. We note the existence of significant torque peaks around the final steady state for the VC-PI control. Then under the VC-STSMC method, we observe a good tracking of both speeds with small oscillations as shown in Figure 16(c), and plots (a) and (b) in Figure 16 show that the torques exhibit peaks around the initial steady state.

Remark: the main objective of the scenario is to test the robustness of the suggested vector control strategy based on second order STSMC under a faulty mode described by one open phase for each machine. Thus, the obtained results confirm that the latter control strategy offers acceptable performance in terms of speed tracking. However, in order to guarantee better performance under faulty modes, fault tolerant control techniques for FP-PMSMs will be applied in our future work. Furthermore, the fault diagnosis and fault location of closed loop feedback systems is a challenging problem. There has been recent and important research work about fault diagnosis that presents very interesting results for readers [57], [58], [59]. In [58], the authors applied a new causality-based technique for the fault diagnosis of a closed-loop feedback control system with multiple modular redundancies to a subsea blowout preventer system. In the field of the subsea production system the authors of [59] proposed a digital twin-driven fault diagnosis method for composite faults. Moreover, an interesting methodology for

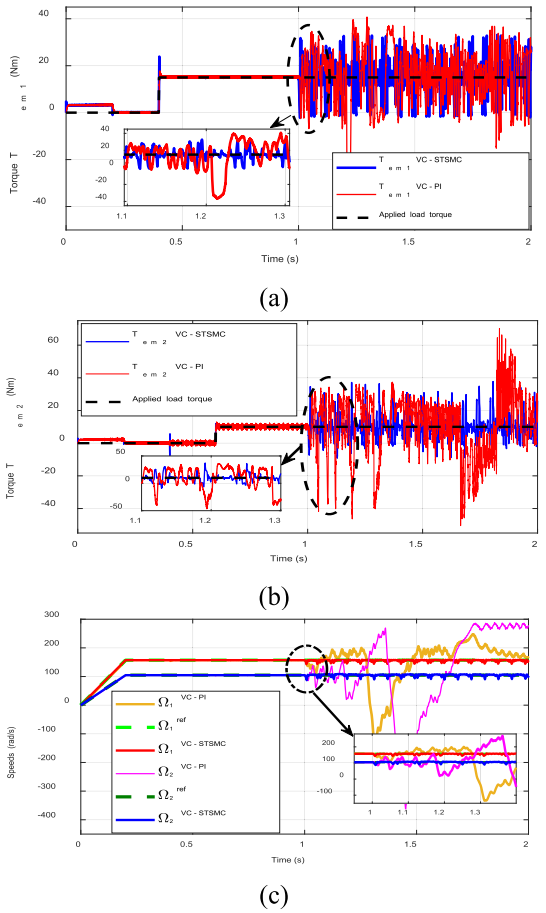

FIGURE 16. Simulation results of torques and speeds under VC-PI control and VC-STSMC in presence of stator phase opening fault: (a) Electromagnetic torques and load torque for FP-PMSM1; (b) Electromagnetic torques and load torque for FP-PMSM2, (c) Real speed responses of two machines.

sensor placement for fault diagnosis of a hydraulic control system was put forward in [57]. The latter method used a discrete particle swarm algorithm for choosing the best positions and the optimal number of sensors that were used to collect fault signals. In the same context, the aforementioned fault diagnosis methods and other recent methodologies will be the main subject of our future research work for series connected PF-PMSMs used for training electrical vehicles.

V. CONCLUSION

In this paper, a robust vector control strategy based on second order STSMC and ST-LTOs for two series-connected FP-PMSMs supplied by a single five-leg inverter is developed. Thus, the major findings in the present work are summarized as follows:

– Firstly, in order to reduce the system cost and the power losses, a conventional vector control strategy based on proportional integral controllers is developed for controlling two series-connected FP-PMSMs supplied by a single five-leg inverter instead of two inverters for the two machines.

– Secondly, for enhancing the performance of the conventional vector control strategy of the two series-connected FP-PMSMs, a novel modified vector control method based on second order STSMCs is carried out. According to the Lyapunov theory, the stability of the proposed controllers is guaranteed. Moreover, and in order to reduce the system cost and the maintenance rate, ST-LTOs are synthesized for estimating the load torque required by the STSMC of speeds.

The simulation results under different operating scenarios in healthy and faulty modes are carried out to improve the performance of the proposed vector control method based on second order STSMC and ST-LTOs. These conditions include load disturbances, stator resistance variations in both machines, high, low and reversal speed operations, and a faulty mode described by one open phase. Indeed, the simulation results show for the FP-PMSM$_1$ that when the conventional vector control method is employed, the average of the total harmonic distortion and the torque ripples are approximately 5.16% and 10.73%, respectively. On the other hand, when the proposed second order STSMC is used, the total harmonic distortion and the torque ripples are 0.32% and 5.98%, respectively. Consequently, reduces the power losses and the mechanical vibrations and increases the FP-PMSM service life. Moreover, when the stator increases, the speed overshoot is evaluated by 1.4% when the conventional vector control method is employed and 0.12% when the proposed second order STSMC is used. In addition, the performance of the suggested vector control method based on second order STSMC is tested under an open phase when the rotor speeds for the two FP-PMSMs present neglected oscillations around their references, whereas the rotor speeds diverge from their references when the conventional vector control strategy is used. This proves the robustness of the suggested control method under parameter variations and such a fault. We have also used other indicators which are the integral of absolute error, the integral of squared error and the integral of time multiplied by the absolute error. In fact, it can be noticed for FP-PMSM$_1$ that for the second order STSMC we have gained 99.69 %, 99.73 % and 99.95 %. More quantitative indicators are presented in the tables of the simulation section, which demonstrate the high performance provided by the suggested control method.

Finally, the results confirm that the STSMCs strategy developed in this study represents a very attractive and promising alternative for high-performance multi-phase machines. Nevertheless, each control method has benefits and limitations, So there are other challenges that remain to be solved in our future work: (*i*) In the future, the proposed methodology will be validated by means of an experimental test bench and can be applied to electrical vehicle applications. *(ii)* The extension of the suggested control algorithm can to be a fault-tolerant control technique in some fault conditions. *(iii)* The recent fault diagnosis method can be applied to the proposed topology based on series connected FP-PMSMs.

APPENDIX

A. GENERALIZED CONCORDIA TRANSFORM

[C] is the power invariant transformation matrix.

$$[C_5] = \sqrt{\frac{2}{5}} \begin{pmatrix} 1 & cos(\frac{2\pi}{5}) & cos(\frac{4\pi}{5}) & cos(\frac{6\pi}{5}) & cos(\frac{8\pi}{5}) \\ 0 & sin(\frac{2\pi}{5}) & sin(\frac{4\pi}{5}) & sin(\frac{6\pi}{5}) & sin(\frac{8\pi}{5}) \\ 1 & cos(\frac{4\pi}{5}) & cos(\frac{8\pi}{5}) & cos(\frac{2\pi}{5}) & cos(\frac{6\pi}{5}) \\ 0 & sin(\frac{4\pi}{5}) & sin(\frac{8\pi}{5}) & sin(\frac{2\pi}{5}) & sin(\frac{6\pi}{5}) \\ \frac{1}{\sqrt{2}} & \frac{1}{\sqrt{2}} & \frac{1}{\sqrt{2}} & \frac{1}{\sqrt{2}} & \frac{1}{\sqrt{2}} \end{pmatrix} \quad (66)$$

B. DATA OF SIMULATION MACHINES

TABLE 4. FP-PMSM1 and FP-PMSM2 parameters.

	Machine parameters	
	FP-PMSM$_1$	FP-PMSM$_2$
Power / Speed	P= 1500 W/ N_n= 1500 rpm	P= 1500 W/ N_n= 1500 rpm
Stator resistance	Rs_1= 2.24 Ω	Rs_2= 2.24 Ω
Cyclic inductance	L_p = 3.2 mH L_s= 0.93 mH	L_p = 3.2 mH L_s= 0.93 mH
Rotor flux	Φ_{F1} = 0.16 Wb	Φ_{F2} = 0.16 wb
Moment of inertia	J_1=0.004 Kg/m^2	J_2=0.004 Kg/m^2
Number of pair poles (P)	2	2

TABLE 5. The relationship betweenξ and $\omega_0 t_{rep}$.

Symbol	ξ	$\omega_0 t_{rep}$
	0.4	7.7
	0.5	5.3
	0.6	5.2
	0.7	3
	1	4.75

TABLE 6. Gains of control strategies.

Controller	Gain	Values
VC -PI	K_{pv} K_{iv}	3.9762 248.6374
	K_{ii} K_{pi} k_i	42.200 38.6207 10
VC -STSMC	k_1, k_{12} k_2, k_3, k_4, k_5	0.100 100
	m_1, m_{12} m_2, m_3, m_4, m_5	12000 600000
ST-LTO	λ_1	20
	$\lambda_2(w)$	100

REFERENCES

[1] R. M. Pindoriya, B. S. Rajpurohit, R. Kumar, and K. N. Srivastava, "Comparative analysis of permanent magnet motors and switched reluctance motors capabilities for electric and hybrid electric vehicles," in *Proc. IEEMA Engineer Infinite Conf. (eTechNxT)*, Mar. 2018, pp. 1–5.

[2] T. J. dos Santos Moraes, M. Trabelsi, N. K. Nguyen, E. Semail, F. Meinguet, and M. Guerin, "Inverter open circuit faults diagnosis in series-connected six-phases permanent magnet drive," in *Proc. IEEE 11th Int. Symp. Diag. Electr. Mach., Power Electron. Drives (SDEMPED)*, Aug. 2017, pp. 188–194.

[3] V. I. Patel, J. Wang, W. Wang, and X. Chen, "Six-phase fractional-slot-per-pole-per-Phase permanent-magnet machines with low space harmonics for electric vehicle application," *IEEE Trans. Ind. Appl.*, vol. 50, no. 4, pp. 2554–2563, Jul. 2014.

[4] G. Mirzaeva, D. Miller, S. Mitchell, and A. Steber, "Hybrid propulsion system for marine vessels based on a DC microgrid," in *Proc. IEEE Energy Convers. Congr. Expo. (ECCE)*, Oct. 2022, pp. 1–7.

[5] T. Bringezu and J. Biela, "Comparison of optimized motor-inverter systems using a stacked polyphase bridge converter combined with a 3-, 6-, 9-, or 12-phase PMSM," in *Proc. 22nd Eur. Conf. Power Electron. Appl. (EPE ECCE Europe)*, Sep. 2020, pp. P.1–P.11.

[6] B. Tian, Q.-T. An, J.-D. Duan, D.-Y. Sun, L. Sun, and D. Semenov, "Decoupled modeling and nonlinear speed control for five-phase PM motor under single-phase open fault," *IEEE Trans. Power Electron.*, vol. 32, no. 7, pp. 5473–5486, Jul. 2017.

[7] T. Zhao, S. Wu, and S. Cui, "Multiphase PMSM with asymmetric windings for more electric aircraft," *IEEE Trans. Transport. Electrific.*, vol. 6, no. 4, pp. 1592–1602, Dec. 2020.

[8] F. Mekri, J.-F. Charpentier, and E. Semail, "An efficient control of a series connected two-synchronous motor 5-phase with non sinusoidal EMF supplied by a single 5-leg VSI: Experimental and theoretical investigations," *Electr. Power Syst. Res.*, vol. 92, pp. 11–19, Nov. 2012.

[9] N. R. Abjadi, "Sliding-mode control of a six-phase series/parallel connected two induction motors drive," *ISA Trans.*, vol. 53, no. 6, pp. 1847–1856, Nov. 2014.

[10] G. Sun, G. Yang, J. Su, and G. Lu, "A flux–linkage torque ripple suppression method of dual–series FPMSMs decoupling control based on dual–frequency vector modulation," *Energies*, vol. 15, no. 13, p. 4700, Jun. 2022.

[11] T. Kamel, D. Abdelkader, B. Said, M. Al-Hitmi, and A. Iqbal, "Sliding mode control based DTC of sensorless parallel-connected two five-phase PMSM drive system," *J. Electr. Eng. Technol.*, vol. 13, no. 3, pp. 1185–1201, 2018.

[12] M. Jones, S. N. Vukosavic, and E. Levi, "Parallel-connected multiphase multidrive systems with single inverter supply," *IEEE Trans. Ind. Electron.*, vol. 56, no. 6, pp. 2047–2057, Jun. 2009.

[13] T. Kamel, D. Abdelkader, B. Said, S. Padmanaban, and A. Iqbal, "Extended Kalman filter based sliding mode control of parallel-connected two five-phase PMSM drive system," *Electronics*, vol. 7, no. 2, p. 14, Jan. 2018.

[14] E. Levi, M. Jones, S. N. Vukosavic, A. Iqbal, and H. A. Toliyat, "Modeling, control, and experimental investigation of a five-phase series-connected two-motor drive with single inverter supply," *IEEE Trans. Ind. Electron.*, vol. 54, no. 3, pp. 1504–1516, Jun. 2007.

[15] Y. Geng, Z. Lai, Y. Li, D. Wang, R. Chen, and P. Zheng, "Sensorless fault-tolerant control strategy of six-phase induction machine based on harmonic suppression and sliding mode observer," *IEEE Access*, vol. 7, pp. 110086–110102, 2019.

[16] A. Hosseyni, R. Trabelsi, M. F. Mimouni, and A. Iqbal, "Vector controlled five-phase permanent magnet synchronous motor drive," in *Proc. IEEE 23rd Int. Symp. Ind. Electron. (ISIE)*, Jun. 2014, pp. 2122–2127.

[17] Z. Li, S. Zhou, Y. Xiao, and L. Wang, "Sensorless vector control of permanent magnet synchronous linear motor based on self-adaptive super-twisting sliding mode controller," *IEEE Access*, vol. 7, pp. 44998–45011, 2019.

[18] M. Hermassi, S. Krim, Y. Kraiem, M. A. Hajjaji, B. M. Alshammari, H. Alsaif, A. S. Alshammari, and T. Guesmi, "Design of vector control strategies based on fuzzy gain scheduling PID controllers for a grid-connected wind energy conversion system: Hardware FPGA-in-the-loop verification," *Electronics*, vol. 12, no. 6, p. 1419, Mar. 2023.

[19] S. Krim and M. F. Mimouni, "Design and Xilinx Virtex-field-programmable gate array for hardware in the loop of sensorless second-order sliding mode control and model reference adaptive system–sliding mode observer for direct torque control of induction motor drive," *Proc. Inst. Mech. Eng. I, J. Syst. Control Eng.*, vol. 237, no. 5, pp. 839–869, May 2023.

[20] H. Wang, G. Buticchi, C. Gu, S. Bai, and M. Galea, "Comparative study of current control techniques for fault-tolerant five-phase PMSM," in *Proc. 47th Annu. Conf. IEEE Ind. Electron. Soc. (IECON)*, Oct. 2021, pp. 1–6.

[21] X. Jin, Q. Wang, Z. Yan, and H. Yang, "Nonlinear robust control of trajectory-following for autonomous ground electric vehicles with active front steering system," *AIMS Math.*, vol. 8, no. 5, pp. 11151–11179, 2023.

[22] X. Jin, J. Wang, H. He, Z. Yan, L. Xu, C. Wei, and G. Yin, "Improving vibration performance of electric vehicles based on in-wheel motor-active suspension system via robust finite frequency control," *IEEE Trans. Intell. Transp. Syst.*, vol. 24, no. 2, pp. 1631–1643, Feb. 2023.

[23] X. Jin, J. Wang, Z. Yan, L. Xu, G. Yin, and N. Chen, "Robust vibration control for active suspension system of in-wheel-motor-driven electric vehicle via μ-synthesis methodology," *J. Dyn. Syst., Meas., Control*, vol. 144, no. 5, May 2022, Art. no. 051007.

[24] T. H. Nguyen, T. T. Nguyen, K. Minh Le, H. N. Tran, and J. W. Jeon, "An adaptive backstepping sliding-mode control for improving position tracking of a permanent-magnet synchronous motor with a nonlinear disturbance observer," *IEEE Access*, vol. 11, pp. 19173–19185, 2023.

[25] L. Sheng, G. Xiaojie, and Z. Lanyong, "Robust adaptive backstepping sliding mode control for six-phase permanent magnet synchronous motor using recurrent wavelet fuzzy neural network," *IEEE Access*, vol. 5, pp. 14502–14515, 2017.

[26] A. Ammar, A. Bourek, and A. Benakcha, "Nonlinear SVM-DTC for induction motor drive using input–output feedback linearization and high order sliding mode control," *ISA Trans.*, vol. 67, pp. 428–442, Mar. 2017.

[27] C. Chen, Y. Song, Y. Zhang, J. Tian, S. Gao, and B. Lang, "Adaptive fault-tolerant control of five-phase permanent magnet synchronous motor current using chaotic-particle swarm optimization," *Frontiers Energy Res.*, vol. 10, Sep. 2022, Art. no. 994629.

[28] W. Liu, S. Chen, and H. Huang, "Adaptive nonsingular fast terminal sliding mode control for permanent magnet synchronous motor based on disturbance observer," *IEEE Access*, vol. 7, pp. 153791–153798, 2019.

[29] J. Longfei, H. Yuping, Z. Jigui, C. Jing, T. Yunfei, and L. Pengfei, "Fuzzy sliding mode control of permanent magnet synchronous motor based on the integral sliding mode surface," in *Proc. 22nd Int. Conf. Electr. Mach. Syst. (ICEMS)*, Aug. 2019, pp. 1–6.

[30] X. Zhang, L. Sun, K. Zhao, and L. Sun, "Nonlinear speed control for PMSM system using sliding-mode control and disturbance compensation techniques," *IEEE Trans. Power Electron.*, vol. 28, no. 3, pp. 1358–1365, Mar. 2013.

[31] L.-B. Li, L.-L. Sun, S.-Z. Zhang, and Q.-Q. Yang, "Speed tracking and synchronization of multiple motors using ring coupling control and adaptive sliding mode control," *ISA Trans.*, vol. 58, pp. 635–649, Sep. 2015.

[32] F.-J. Lin, Y.-C. Hung, and M.-T. Tsai, "Fault-tolerant control for six-phase PMSM drive system via intelligent complementary sliding-mode control using TSKFNN-AMF," *IEEE Trans. Ind. Electron.*, vol. 60, no. 12, pp. 5747–5762, Dec. 2013.

[33] B. Tian, G. Mirzaeva, Q.-T. An, L. Sun, and D. Semenov, "Fault-tolerant control of a five-phase permanent magnet synchronous motor for industry applications," *IEEE Trans. Ind. Appl.*, vol. 54, no. 4, pp. 3943–3952, Jul. 2018.

[34] A. Hosseyni, R. Trabelsi, A. Iqbal, and M. F. Mimouni, "Comparative study of adaptive sliding mode and resonant controllers in fault tolerant five-phase permanent magnet synchronous motor drive," *Int. J. Adv. Manuf. Technol.*, vol. 96, nos. 5–8, pp. 2195–2213, May 2018.

[35] C. Gong, Y. Hu, J. Gao, Y. Wang, and L. Yan, "An improved delay-suppressed sliding-mode observer for sensorless vector-controlled PMSM," *IEEE Trans. Ind. Electron.*, vol. 67, no. 7, pp. 5913–5923, Jul. 2020.

[36] N. Bounasla, S. Barkat, E. Benyoussef, and K. Tounsi, "Sensorless sliding mode control of a five-phase PMSM using extended Kalman filter," in *Proc. 8th Int. Conf. Model., Identificat. Control (ICMIC)*, Nov. 2016, pp. 97–102.

[37] A. Chihi, H. Ben Azza, M. Jemli, and A. Sellami, "Nonlinear integral sliding mode control design of photovoltaic pumping system: Real time implementation," *ISA Trans.*, vol. 70, pp. 475–485, Sep. 2017.

[38] F. Mehedi, L. Nezli, M. O. Mahmoudi, and A. B. Djilali, "A hybrid of sliding mode control and fuzzy logic control for a five-phase synchronous motor speed control," in *Renewable Energy for Smart and Sustainable Cities: Artificial Intelligence in Renewable Energetic Systems*, vol. 2. Cham, Switzerland: Springer, 2019, pp. 199–205.

[39] B. Bouchiba, I. K. Bousserhane, M. K. Fellah, and A. Hazzab, "Artificial neural network sliding mode control for multi-machine web winding system," *Revue Roumaine des Sci. Techn. Série Électrotechnique et Énergétique*, vol. 62, pp. 109–113, Apr. 2017.

[40] K. Sahraoui, K. Kouzi, and A. Ameur, "Neural networks trained with sliding mode control for DSIM supplied by two voltage inverters on three levels," in *Proc. Int. Conf. Electr. Sci. Technol. Maghreb (CISTEM)*, Oct. 2018, pp. 1–6.

[41] Q. Wang, H. Yu, M. Wang, and X. Qi, "An improved sliding mode control using disturbance torque observer for permanent magnet synchronous motor," *IEEE Access*, vol. 7, pp. 36691–36701, 2019.

[42] Y. Zahraoui, F. M. Zaihidee, M. Kermadi, S. Mekhilef, I. Alhamrouni, M. Seyedmahmoudian, and A. Stojcevski, "Optimal tuning of fractional order sliding mode controller for PMSM speed using neural network with reinforcement learning," *Energies*, vol. 16, no. 11, p. 4353, May 2023.

[43] A. Levant, "Sliding order and sliding accuracy in sliding mode control," *Int. J. Control*, vol. 58, no. 6, pp. 1247–1263, Dec. 1993.

[44] M. Ayadi, O. Naifar, and N. Derbel, "High-order sliding mode control for variable speed PMSG-wind turbine-based disturbance observer," *Int. J. Model., Identificat. Control*, vol. 32, no. 1, pp. 85–92, 2019.

[45] Y. Zafari, and S. Shoja-Majidabad, "Second-order terminal sliding mode control of five-phase IPMSM with super twisting observer under demagnetisation fault," *Int. J. Model., Identificat. Control*, vol. 34, no. 2, pp. 127–136, 2020.

[46] L. Li, L. Sun, and S. Zhang, "Mean deviation coupling synchronous control for multiple motors via second-order adaptive sliding mode control," *ISA Trans.*, vol. 62, pp. 222–235, May 2016.

[47] S. Di Gennaro, J. R. Domínguez, and M. A. Meza, "Sensorless high order sliding mode control of induction motors with core loss," *IEEE Trans. Ind. Electron.*, vol. 61, no. 6, pp. 2678–2689, Jun. 2014.

[48] A. Chalanga, S. Kamal, L. M. Fridman, B. Bandyopadhyay, and J. A. Moreno, "Implementation of super-twisting control: Super-twisting and higher order sliding-mode observer-based approaches," *IEEE Trans. Ind. Electron.*, vol. 63, no. 6, pp. 3677–3685, Jun. 2016.

[49] M. Hu, H. Ahn, Y. Chung, and K. You, "Speed regulation for PMSM with super-twisting sliding-mode controller via disturbance observer," *Mathematics*, vol. 11, no. 7, p. 1618, Mar. 2023.

[50] J. Chen, Z. Shuai, H. Zhang, and W. Zhao, "Path following control of autonomous four-wheel-independent-drive electric vehicles via second-order sliding mode and nonlinear disturbance observer techniques," *IEEE Trans. Ind. Electron.*, vol. 68, no. 3, pp. 2460–2469, Mar. 2021.

[51] F. Bonnet, "Contribution à l'optimisation de la commande d'une machine synchrone à double alimentation utilisée en mode moteur," Doctorat De, Nat. Polytech. Inst. Toulouse, L'Universite De Toulouse, Toulouse, France, 2008.

[52] A. Lokriti, Y. Zidani, and S. Doubabi, "Comparaison des performances des régulateurs PI et IP appliques pour la commande vectorielle a flux rotorique oriente d'une machine asynchrone," in *Proc. 8th Int. IFAC Conf. Model. Simulation (MOSIM)*, May 2010, pp. 1–7.

[53] D. Xu, S. Zhang, and J. Liu, "Very-low speed control of PMSM based on EKF estimation with closed loop optimized parameters," *ISA Trans.*, vol. 52, no. 6, pp. 835–843, 2013.

[54] S. D. Gennaro, J. Rivera, and B. Castillo-Toledo, "Super-twisting sensorless control of permanent magnet synchronous motors," in *Proc. 49th IEEE Conf. Decis. Control (CDC)*, Atlanta, GA, USA, Dec. 2010, pp. 4018–4023.

[55] I. Sami, S. Ullah, A. Basit, N. Ullah, and J.-S. Ro, "Integral super twisting sliding mode based sensorless predictive torque control of induction motor," *IEEE Access*, vol. 8, pp. 186740–186755, 2020.

[56] J. Gil, S. You, Y. Lee, and W. Kim, "Super twisting-based nonlinear gain sliding mode controller for position control of permanent-magnet synchronous motors," *IEEE Access*, vol. 9, pp. 142060–142070, 2021.

[57] X. Kong, B. Cai, Y. Liu, H. Zhu, Y. Liu, H. Shao, C. Yang, H. Li, and T. Mo, "Optimal sensor placement methodology of hydraulic control system for fault diagnosis," *Mech. Syst. Signal Process.*, vol. 174, Jul. 2022, Art. no. 109069.

[58] X. Kong, B. Cai, Y. Liu, H. Zhu, C. Yang, C. Gao, Y. Liu, Z. Liu, and R. Ji, "Fault diagnosis methodology of redundant closed-loop feedback control systems: Subsea blowout preventer system as a case study," *IEEE Trans. Syst., Man, Cybern., Syst.*, vol. 53, no. 3, pp. 1618–1629, 2022.

[59] C. Yang, B. Cai, Q. Wu, C. Wang, W. Ge, Z. Hu, W. Zhu, L. Zhang, and L. Wang, "Digital twin-driven fault diagnosis method for composite faults by combining virtual and real data," *J. Ind. Inf. Integr.*, vol. 33, Jun. 2023, Art. no. 100469.

ALI AJMI received the Master of Science and Master of Research degrees from ESST, Tunisia, in 1995 and 2004, respectively. He is currently pursuing the Ph.D. degree with the University of Monastir, Tunisia. He is a member of the Laboratory of Automatic, Electrical Systems and Environment (LASEE), National Engineering School of Monastir, University of Monastir. He is a Teacher with the Higher Institute of Technological Studies of Sousse, Tunisia. His current research interests include the modeling and control of multiphase motor drives.

SABER KRIM received the Electrical Engineering Diploma, master's, and Ph.D. degrees in electrical engineering from the National Engineering School of Monastir, University of Monastir, Tunisia, in 2011, 2013, and 2017, respectively. He is currently an Assistant Professor of electrical engineering with the Technology Department, Higher Institute of Applied Sciences and Technologies of Kasserine, University of Kairouan, Kairouan, Tunisia. He is a member of the Laboratory of Automatic, Electrical Systems and Environment (LASEE), National Engineering School of Monastir, University of Monastir. He has authored/coauthored over 50 papers in international journals and conferences. His current research interests include rapid prototyping and reconfigurable architecture for real-time control applications of electrical systems, power electronics, motor drives, and solar and wind power generation.

ANISSA HOSSEYNI received the Electrical Engineering Diploma, master's, and Ph.D. degrees in electrical engineering from the National Engineering School of Monastir, University of Monastir, Tunisia, in 2011, 2013, and 2018, respectively. She is currently a member of the Laboratory of Automatic, Electrical Systems and Environment (LASEE), National Engineering School of Monastir, University of Monastir. She has authored 11 papers in international journals and conferences. Her research interests include the modeling and control of multiphase motor drives.

MAJDI MANSOURI (Senior Member, IEEE) received the degree in electrical engineering from SUPCOM, Tunis, Tunisia, in 2006, the M.Sc. degree in electrical engineering from ENSEIRB, Bordeaux, France, in 2008, the Ph.D. degree in electrical engineering from UTT Troyes, France, in 2011, and the H.D.R. (Accreditation To Supervise Research) degree in electrical engineering from the University of Orleans, France, in 2019. He joined the Electrical Engineering Program, Texas A&M University at Qatar, in 2011, where he is currently an Associate Research Scientist. He is the author of more than 200 publications. He is also the author of the book *Data-Driven and Model-Based Methods for Fault Detection and Diagnosis* (Elsevier, 2020). His research interests include development of model-based, data-driven, and machine learning techniques for fault detection and diagnosis.

MOHAMED FAOUZI MIMOUNI received the Master of Science, DEA, and Ph.D. degrees in electrical engineering from ENSET, Tunisia, in 1984, 1986, and 1997, respectively. He is currently a Full Professor of electrical engineering with the Electrical Department, National Engineering School of Monastir. He has authored/coauthored over 100 papers in international journals and conferences. His research interests include power electronics, motor drives, and solar and wind power generation. He served on the technical program committees for several international conferences.

Open Access funding provided by 'Qatar National Library' within the CRUI CARE Agreement